J. Cell. Mol. Med. Vol 16, No 7, 2012 pp. 1629-1639

Modification of a novel angiogenic peptide, AG30, for the development of novel therapeutic agents

Hironori Nakagami [a, b, *], Tomoyuki Nishikawa [a], Nao Tamura [c], Akito Maeda [d], Hajime Hibino [e], Masayoshi Mochizuki [e], Takashi Shimosato [f], Toshinori Moriya [f], Ryuichi Morishita [g], Katsuto Tamai [a], Kazunori Tomono [h], Yasufumi Kaneda [a, *]

[a] *Division of Gene Therapy Science, Osaka University Graduate School of Medicine, Suita, Osaka, Japan*
[b] *Division of Vascular Medicine and Epigenetics, Osaka University United Graduate School of Child Development, 2-1 Yamada-oka, Suita, Osaka, Japan*
[c] *Anges-MG, Inc. 7-7-15 Saito Bio-Incubator, Ibaraki, Osaka, Japan*
[d] *Skin Regeneration, PIAS Collaborative Research, The Center for Advanced Science and Innovation, Osaka University, Osaka, Japan*
[e] *Peptide Institute, Inc. 7-2-9 Saito Asagi, Ibaraki, Osaka, Japan*
[f] *Research Department, NISSEI BILIS Co. Ltd., Koka, Shiga, Japan*
[g] *Department of Clinical Gene Therapy, Osaka University Graduate School of Medicine, Suita, Osaka, Japan*
[h] *Division of Infection Control and Prevention, Osaka University Graduate School of Medicine, Suita, Osaka, Japan*

Received: February 12, 2011; Accepted: July 28, 2011

Abstract

We previously identified a novel angiogenic peptide, AG30, with antibacterial effects that could serve as a foundation molecule for the design of wound-healing drugs. Toward clinical application, in this study we have developed a modified version of the AG30 peptide characterized by improved antibacterial and angiogenic action, thus establishing a lead compound for a feasibility study. Because AG30 has an α-helix structure with a number of hydrophobic and cationic amino acids, we designed a modified AG30 peptide by replacing several of the amino acids. The replacement of cationic amino acids (yielding a new molecule, AG30/5C), but not hydrophobic amino acids, increased both the angiogenic and the antimicrobial properties of the peptide. AG30/5C was also effective against *methicillin-resistant Staphylococcus aureus* (MRSA) and antibiotic-resistant *Pseudomonas aeruginosa*. In a diabetic mouse wound-healing model, the topical application of AG30/5C accelerated wound healing with increased angiogenesis and attenuated MRSA infection. To facilitate the eventual clinical investigation/application of these compounds, we developed a large-scale procedure for the synthesis of AG30/5C that employed the conventional solution method and met Good Manufacturing Practice guidelines. In the evaluation of stability of this peptide in saline solution, RP-HPLC analysis revealed that AG30/5C was fairly stable under 5°C for 12 months. Therefore, we propose the use of AG30/5C as a wound-healing drug with antibacterial and angiogenic actions.

Keyword: angiogenesis • antimicrobial • translational research • drug development

Introduction

Antimicrobial peptides are small proteins that are used by the innate immune system to combat bacterial infections in multicellular eukaryotes. The emergence of drug-resistant bacteria has driven the extensive investigation of these peptides as a potential source of new antimicrobial drugs that could complement current antibiotic regimes [1, 2]. In general, antimicrobial peptides are characterized by a net positive charge and an amphipathic three-dimensional structure that gives the peptides an electrostatic affinity to the outer leaflet of the microbial membrane, mediated by lipid molecules on bacterial surfaces [3]. This affinity leads to binding, disruption of the membrane and microbial cell death [4]. More than 100 antimicrobial peptides have been discovered in animals ranging from insects to humans; however, the development of antimicrobial peptide-based

*Correspondence to: Hironori NAKAGAMI, M.D., Ph.D.,
Yasufumi KANEDA, M.D., Ph.D.,
Division of Gene Therapy Science,
Graduate School of Medicine, Osaka University,
2-2 Yamada-oka, Suita 565–0871, Japan.
Tel.: +81-6-6879-3901
Fax: +81-6-6879-3909
E-mail: nakagami@gts.med.osaka-u.ac.jp, kaneday@gts.med.osaka-u.ac.jp

doi:10.1111/j.1582-4934.2011.01406.x

therapies has mainly been restricted to topical or local treatments because their activity is suppressed in serum [3–5].

We recently developed a novel antimicrobial peptide, named AG30, with angiogenic properties potentially similar to those of LL37 or PR39 [6]. Because both angiogenic and antimicrobial effects are beneficial in the process of wound healing, we initiated the clinical development process using AG30 as a foundation compound to develop novel topically applied wound-healing drugs. The development of a peptide-drug based topical treatment has several attractive features: (1) the drug is delivered directly to the wound; (2) high local tissue levels can be achieved through application of aggressive doses; and (3) the short half life of peptides, resulting from their degradation by peptidases, reduces their toxicity. Historically, similar cationic antimicrobial peptides, such as pexiganan, iseganan and omiganan, failed to pass the phase II or III trials in topical applications or systemic applications. Therefore, in this study, we developed the load compound based on a feasibility study using the foundation compound, AG30. Using both *in silico* and functional analyses, we produced a modified version of the AG30 peptide that may elicit more potent angiogenic and antimicrobial effects. As initial steps in the investigation of the potential clinical applications of this modified AG30 peptide, we developed a cost-effective production process and evaluated its efficiency using animal models.

Material and methods

Cell migration assay and tube formation assays and cell growth assay

Human aortic endothelial cells (HAEC, passage 3) were purchased from Clonetics Corp. (Palo Alto, CA, USA) and maintained in endothelial basal medium (EBM-2) that was supplemented with 5% foetal bovine serum (FBS) and endothelial growth supplement as described previously [6]. Cells were incubated at 37°C in a humidified atmosphere of 95% air–5% CO_2 with exchange of medium every 2 days.

Human aortic endothelial cells migration was assayed using a modified Boyden chamber, as previously described [7]. Human aortic endothelial cells tube formation assays were conducted in triplicate in 24-well plates using an Angiogenesis Kit (Kurabo, Osaka, Japan) according to the manufacturer's instructions, as previously described [6].

Human epidermal keratinocytes cell line (HaCaT cells) were maintained with DMEM supplemented with 10% FBS and 10 μg/ml Gentamicin. We used the MTS [3-(4,5-dimethylthiazol-2-yl)-5-(3-carboxymethoxyphenyl)-2-(4-sulfophenyl)-2H- tetrazolium] assay for cell growth. Second day after stimulation with AG30/5C, 10 μl of Cell Riter 96 One Solution Reagent (Progema, Medison, WI, USA) was added to each well, and absorbance at 490 nm was measured [6].

Peptide design and synthesis and circular dichroism (CD) spectroscopy analysis

All peptides used in this experiment were purchased from the Peptide Institute, Inc. (Osaka, Japan). LL37 was synthesized as described previously [8]. The Boman Index was used to predict the function of the peptides [9]. We used the AGADIR program (http://www.embl-heidelberg.de/ExternalInfo/serrano/agadir/agadir-start.html) to predict the structure. Circular dichroism data were acquired with a Jasco J-820 spectrophotometer using a 1-mm-path-length cuvette at 20°C [10]. Spectra were collected for samples containing 0.3 μg/ml peptide in 20 mM phosphate buffer at pH 7.5, with and without the addition of 30% or 60% trifluoroethanol (TFE) [11].

Measurement of MICs against *P. aeruginosa*, *S. aureus* and *Candida*

The minimum inhibitory concentrations (MICs, expressed as μg/ml) of modified AG30 and LL37 for *Psudomonas aeruginosa* (*P. aeruginosa,* ATCC27853), *Staphylolcoccus aureus* (*S. aureus,* ATCC29213) and *Candida albicans* (*Candida*, ATCC90028) and *methicillin-resistant S. aureus* (MRSA) were defined as the lowest concentration of peptide that inhibited visible bacterial growth after incubation for 16 hrs at 37°C with vigorous shaking, as previously described [6]. This experimental protocol was approved by the bio-safety committee at the Osaka University Graduate School of Medicine.

Mouse wound model and infection models

In the mice tail wound model, full-thickness wounds were made on the dorsal surface of mouse tails as previously described [12]. For wound-healing model, 9-week-old male C57BL/6 db/db mice were used in this study. We completely removed hair from the backs of mice using fine-tooth clippers and hair-removing cream 3 days prior to operation. After induction of anaesthesia, 15 mm punch biopsy wounds were made on the backs of each mouse (n = 10–12 in each group). After topical application of each peptide (100 μg/ml), the wounds were covered with a semi-permeable polyurethane dressing. Topical application of each peptide and measurements of wound areas were repeated on days 0, 2, 4, 7, 9, 11, 14 and 16. Samples were obtained 7 days after the operation. After fixation in cold acetone (at −20°C for 15 min.), capillary EC were identified by immunohistochemical staining using an antimouse PECAM mAb (Pharmingen, San Diego, CA, USA) and then counted in 10 independent views of each group [13]. After day 16, peptide application and film dressing were halted for 10 days, and hair growth was observed.

Similar to the mouse wound model, we made wounds on the backs of db/db mice (n = 6–8 in each group). We topically applied 100 μl of methicillin-resistant *S. aureus* on the wounds (1×10^4 cfu/ml) with or without each peptide tested (100 μg/ml). The wounds were then covered with a semi-permeable polyurethane dressing. Topical application of each peptide and measurements of wound areas by taking pictures were repeated on days 0, 2, 4, 7, 9, 11, 14 and 16. All animal experiments were performed according to the Guidelines for Animal Experiments at the Osaka University Graduate School of Medicine.

Measurement of blood flow by Lase Doppler imaging

Measurement of blood flow with Laser Doppler imaging (LDI; Moor Instruments, Axminister, UK) was performed as described previously [13,

14]. Because Laser Doppler flow velocity correlates with capillary density, we measured the blood flow just below the skin by LDI. Consecutive measurements were obtained over the same regions of interest by averaging four sites around the wound.

Porcine wound-healing model

In the porcine wound model, full-thickness wounds were made on the side abdomen surface of pigs as modified previous method [15]. Three male NIBS minipigs (32.0, 32.1 or 33.5 kg) were used (NARC Corporation, Chiba). Pigs were pre-medicated with ketamine (500 mg/body) and isoflurane (2–4%) were administered for anaesthesia. We completely removed hair from the side abdomen of pigs using fine-tooth clippers and outlined the circle in a 25 mm diameter. Full-thickness excisional wounds were created in a uniform depth of 10 mm. We created four wounds on one side at intervals of 30 mm. After topical application (200 μl/site) of each peptide (100 μg/ml), the wounds were covered with a semipermeable polyurethane dressing. Topical application of each peptide was repeated on days 0, 2, 4, 6, 8 and 10. Samples were obtained 12 days after the operation. These frozen sections were stained with haematoxylin and eosin for overall morphological observation. After fixation in cold acetone (at −20°C for 15 min.), capillary EC were identified by immunohistochemical staining with von Willebrand factor (1:200 dilution; DAKO, Glostrup, Denmark) [16]. All animal experiments were performed according to the Guidelines for Animal Experiments at the Osaka University Graduate School of Medicine.

Statistical analysis

All values are expressed as means ± S.E.M. Analysis of variance with subsequent Fisher's PLSD test analysis was used to determine the significance of differences in multiple comparisons.

Results

Development of a modified versions of the AG30 peptide

We previously identified a novel angiogenic peptide consisting of 30 amino acids, named AG30 [6]. As shown in Figure 1A, AG30 is a good foundation molecule for the development of wound-healing drugs, and this study may help to establish the feasibility of AG30-related lead compounds for clinical applications. The original AG30 molecule has an amphipathic structure; most of the positively charged amino acids are localized to one side of the molecule, while most of the hydrophobic amino acids are localized to the opposite side [6]. Notably, AG30 contains very few proline or glycine residues that would interrupt the α-helical structure. Thus, in our design strategy for developing modified AG30 molecules, we replaced several neutral amino acids (specifically proline, asparagine, asparagine acid and serine) with cationic or hydrophobic amino acids and added a capping structure (Ac-KLT on the C-terminus and KGI-amido on the N-terminus) to stabilize the helical structure [15] (Fig. 1B). The total net charge of each designed peptide is increased by adding cationic amino acids (AG30: +11, AG30/2C: +14, AG30/5C: +17, respectively).

We evaluated the potential activity of these candidate peptides using two different types of *in silico* analysis. To predict the structure, we used the AGADIR program, an algorithm based on the helix/coil transition theory that predicts the helical behaviour of monomeric peptides [17, 18]. In this analysis, the addition of five hydrophobic amino acids and a capping structure increased the score, although the addition of two or five cationic amino acids decreased the score (Fig. 1C). The Boman Index [9] was used to predict the function of the peptides; this index is calculated by adding the free energies of the side chains for transfer from cyclohexane to water and dividing that sum by the total number of residues. In this analysis, the addition of cationic amino acids gave a high score, while the addition of hydrophobic amino acids and a capping structure decreased the score (Fig. 1C).

Evaluation of modified AG30 peptides

As an initial evaluation of the designed peptides, we investigated their effects on the migration and tube forming ability of human aortic endothelial cells. In the migration assay, the addition of five cationic amino acids (*i.e.* compound AG30/5C) resulted in increased migration activity; however, the addition of a capping structure (*i.e.* compound AG30+Cap) resulted in a lower activity compared to AG30 (Fig. 1D). In the tube formation assay, the addition of cationic charged or hydrophobic amino acids strongly induced tube formation. However, the addition of a capping structure reduced this activity (Fig. 1E and F). We also examined the antibacterial effects of the designed peptides against *P. aeruginosa*, *Candida* and *S. aureus*. The addition of two or five cationic amino acids (*i.e.* compound AG30/2C or AG30/5C) increased the antibacterial activity against all bacteria, although the addition of five hydrophobic amino acids (*i.e.* compound AG30/5H) resulted in a lower antibacterial activity than AG30 (Fig. 2A–D). These results suggest that the addition of five cationic amino acids (*i.e.* compound AG30/5C) enhances both the angiogenic and the antimicrobial properties of the original AG30 molecule, a result that is compatible with the previously determined Boman Index scores.

In the structural analysis of the peptides using CD spectroscopy, all of the candidate peptides showed negligible helical structure in aqueous buffer; the addition of the helix-inducing cosolvent TFE (either 20% or 60%) resulted in the appearance of a clear helical component. This was demonstrated by the minimums at 208 and 220 nm and the increase of ellipticity at 200 nm, which resulted in the appearance of a clear helical component in all of the generated peptide. But the control peptide did not change upon the addition of TFE. We quantified the helical structure [19] formation tendency of each of the peptides, either with or without TFE (Fig. 3A–F). Unexpectedly, the addition of either five

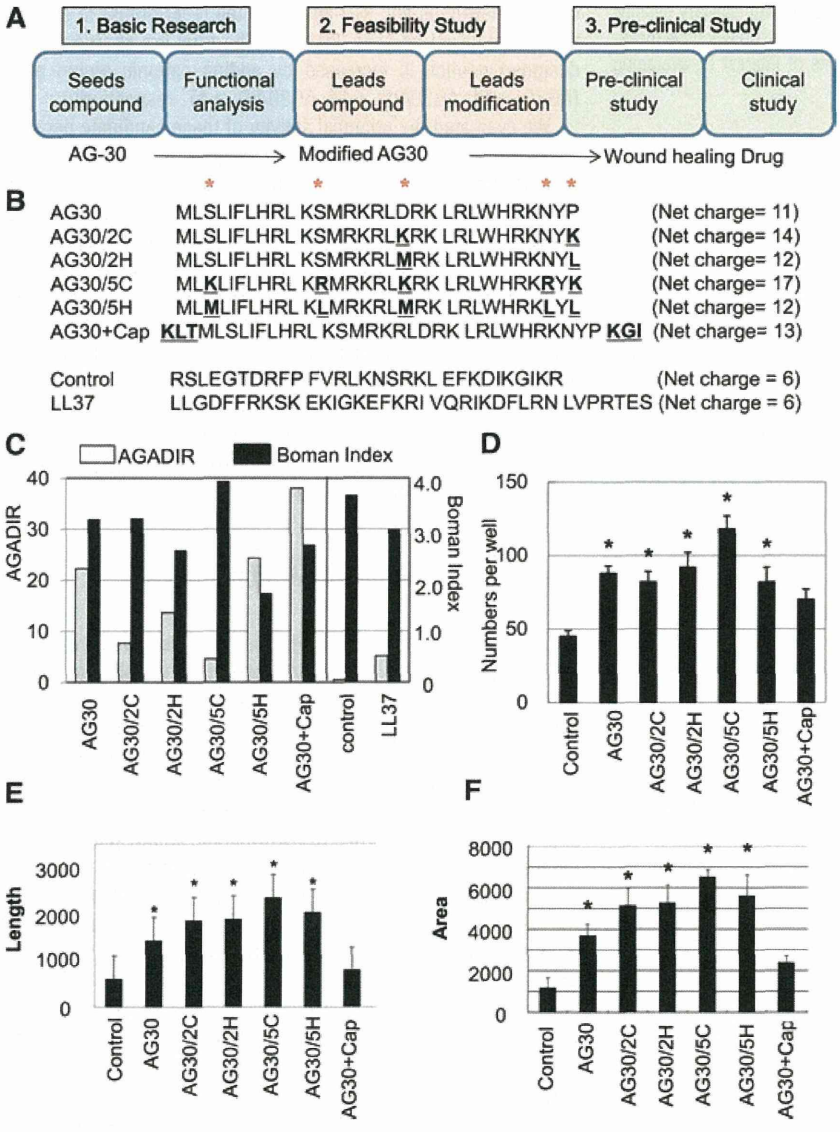

Fig. 1 Several different modified AG30 peptides were created by replacing hydrophobic or cationic amino acids or adding capping structures. (**A**) Study design of this research. AG30 can be a good seed for wound-healing drug and this modified AG30 may correspond to be lead compounds as feasibility study toward clinical application (towards wound-healing drug). (**B**) Peptide sequences and net charge of modified AG30, control peptide and LL37. '*' indicates positions where amino acids were replaced. 'AG30/2C' and 'AG30/5C' indicate the replacement of two or five cationic amino acid (from S, S, D, N, P to K, R, K, R, K, respectively). 'AG30/2H' and 'AG30/5H' indicate the replacement of two or five hydrophobic amino acids (from S, S, D, N, P to M, L, M, L, L, respectively). 'AG30+Cap' indicates the addition of a capping structure (Ac-KLT on the C-terminus and KGI-amide on the N-terminus). (**C**) *In silico* analysis of modified AG30. AGADIR (white bar) scores were calculated to predict the peptide structure and the Boman Index (black bar) was calculated to predict the pleiotropic effects of cationic peptides. (**D**) HAEC migration after treatment with modified AG30 for 24 hrs. (**E**, **F**) Tube formation after daily treatment with modified AG30 for 4 days; length and area were measured. $N = 6$ per group and duplicated. $^{*}P < 0.05$ *versus* control, $^{\dagger}P < 0.05$ *versus* AG30.

hydrophobic amino acids (*i.e.* compound AG30/5H) or a capping structure (*i.e.* compound AG30+Cap) did not increase the ratio of α-helical structures, and the addition of five cationic amino acids (*i.e.* compound AG30/5C) decreased the α-helical structure ratio in comparison to AG30. These results suggest that the ratio of α-helical structures upon the addition of TFE does not correspond to the AGADIR score and thus might not correspond to the angiogenic or antibacterial properties of each peptide. Similarly, the well-known antimicrobial peptide LL37 has a low AGADIR score but was found to possess an α-helical structure without addition of TFE. Furthermore, LL-37 has strong angiogenic effects and a high Boman Index score, indicating that the Boman index is more reliable for *in silico* screening in our study.

Antibacterial effects of modified AG30 (AG30/5C)

The advantage of using antimicrobial peptides as antibacterial agents is that bacteria are less likely to become resistant to these compounds in comparison to antibiotics. Indeed, the antibacterial effects (MICs) of AG30 and AG30/5C against MRSA were similar to their effects against methicillin-sensitive *S. aureus* (Fig. 2C and D).

Thus, we examined the MICs of AG30 and AG30/5C against antibiotic-resistant strains (A–E) of *P. aeruginosa* that were resistant to several types of antibiotics. Notably, AG30 and AG30/5C were both effective against antibiotic-resistant *P. aeruginosa* (Table 1). In this assay, AG30/5C also showed a more powerful antibacterial effect in comparison to the original AG30 peptide. Its

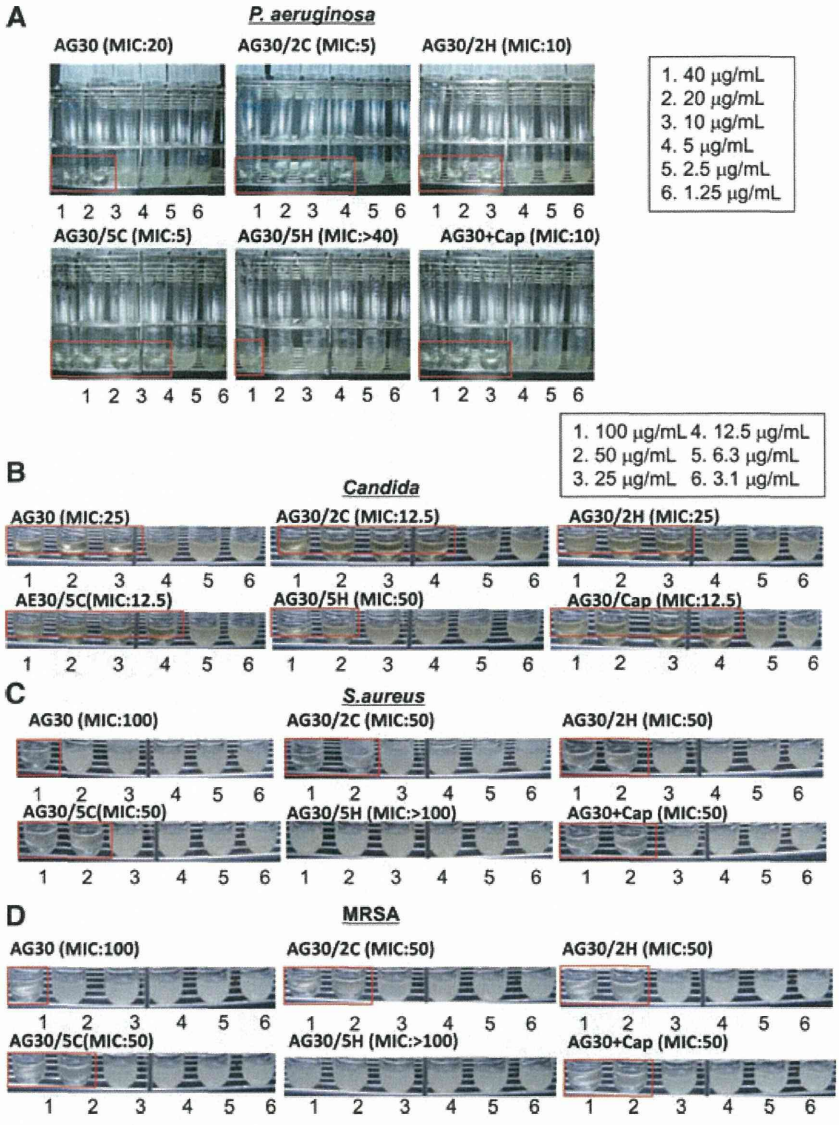

Fig. 2 The antibacterial action of modified AG30. The antibacterial action of modified AG30 is evaluated to (**A**) *P. aeruginosa* (ATCC27853), (**B**) *Candida* (ATCC90028), (**C**) *S. aureus* (ATCC29213) and (**D**) MRSA. MIC assays were performed in the concentration range of 1.25–40 mg/ml of modified AG30, LL37 against *P. aeruginosa* and 3.1–100 mg/ml against *Candida*, *S. aureus* and MRSA. MIC was defined as the lowest peptide concentration, which prevented visible bacterial growth in the medium. Lower panel shows representative pictures of MIC assays with treatment of several peptides.

antibacterial effects might occur through a 'lytic' mechanism that results from the attachment of cationic peptides to the bacterial membrane. To test this idea, we exogenously added cationic ions, such as $CaCl_2$ or $MgCl_2$, and examined whether the antibacterial effect of AG30/5C was inhibited. Indeed, the addition of $CaCl_2$ or $MgCl_2$ (both at 3 and 6 mM) completely blocked the antibacterial effects of AG30/5C (Table 2). These results suggest that AG30/5C kills bacteria through a lysis-based mechanism that may be different from the actions of other antibiotics.

Based on these results, we selected molecules to which five cationic amino acids has been added (*i.e.* compound AG30/5C) as lead compounds for the next stage of investigation and further evaluated the function of AG30/5C.

Development of a production system for modified AG30 (AG30/5C)

To facilitate the eventual clinical investigation/application of these compounds, we developed a large-scale procedure for the synthesis of AG30/5C that employed the conventional solution method and met Good Manufacturing Practice guidelines. The AG30/5C molecule was assembled from four segments, that is (1–10), (11–17), (18–23) and (24–30), as shown in Figure 4A. The carboxyl terminus of each of the segments was protected by a phenacyl ester (Pac) group, except for the C-terminal segment that was instead protected by a benzyl ester group. All of the side-chain functional groups were protected as follows:

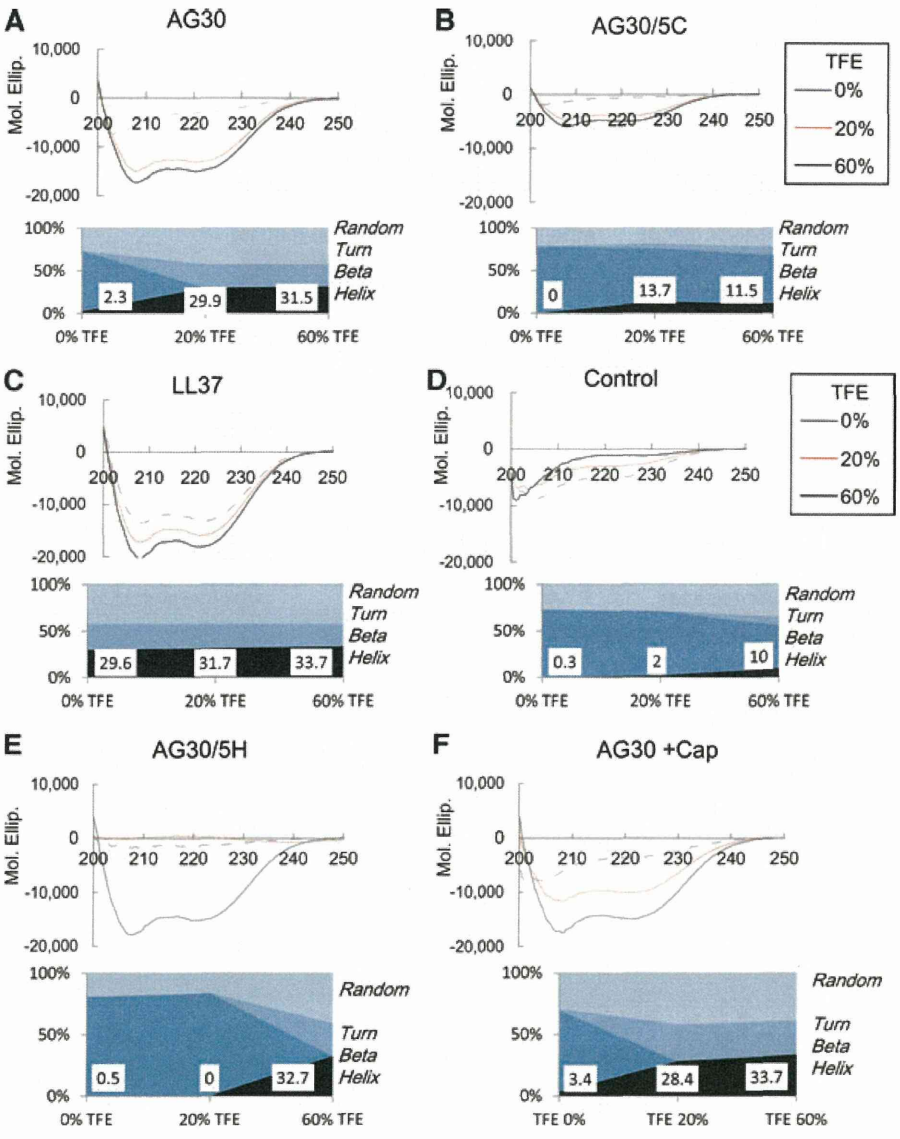

Fig. 3 CD spectroscopy analysis. Modified AG30, LL37 and control peptide showed negligible helical structure in aqueous buffer, and the addition of the helix inducing cosolvent trifluoroethanol (20% or 60%) resulted in the appearance of a clear helical component, that demonstrated the minimum at 208 and 220 nm and the increase of ellipticity at 200 nm. In lower panel, the quantification of helical structure (Random, Turn, Beta, and Helix) was calculated, and the score of helix has been shown.

2-chlorobenzyloxycarbonyl (ClZ) for Lys, benzyloxymethyl (Bom) for His, *p*-toluenesulfonyl (Tos) for Arg, formyl (CHO) for Trp and 2-bromobenzyloxycarbonyl (BrZ) for Tyr. Each segment was elongated stepwise using the EDC/HOBt coupling reagent method. During the chain assembly, the common starting material (*i.e.* Boc-Arg(Tos)-Leu-OPac) could be used for preparing segments (1–10), (11–17) and (18–23) because AG30/5C contains an Arg-Leu sequence at positions 9–10, 16–17 and 22–23. This facilitated the preparation of these segments. Before being subjected to segment condensation reactions, each segment was treated with zinc powder in acetic acid to remove the Pac group from the C-terminus. The C-terminal segment was elongated in a sequential manner with segments containing a free carboxylic acid at the C-terminus by applying the EDC/HOOBt method in DMF to obtain the fully protected AG30/5C peptide. After subsequent removal of the N^{α}-Boc group and the CHO group on Trp using TFA and 10% piperidine/DMF, all of the protecting groups were removed by HF/*p*-cresol (v/v, 85/15) in the presence of methoxyamine·HCl and 2-mercaptopyridine at −2°C to −5°C for 1 hr [17]. After conversion of the peptide from the HF form to the AcOH form using a Muromac (acetate form) column, the crude product was purified by ion-exchange chromatography on a CM-Sepharose column using a gradient of 20 mM $AcONH_4$ buffer to 2 M NaCl/20 mM $AcONH_4$ buffer (pH 5.0). This was followed by RP-HPLC on an YMC-Pak ODS column using a gradient of 20% CH_3CN/0.1% TFA to 40% CH_3CN/0.1% TFA. The purified product was passed

Table 1 MIC of AG30 or AG30/5C to antibiotic-resistant strain (A–E) of *P. aeruginosa*

	A	B	C	D	E
AG30	20	10	40	20	10
AG30/5C	10	5	20	20	10
CAZ	<8: S	<8: S	<8: S	<8: S	>32: R
CFPM	<8: S	<8: S	<8: S	<8: S	>16: R
CPZ	<16: S	32	<16: S	<16: S	>32: R
IPM/CS	<4: S	<4: S	<4: S	>8: R	<4: S
AZT	<8: S	>16: R	<8: S	<8: S	>16: R
TOB	>8: R	<4: S	>8: R	<4: S	<4: S
GM	>8: R	<4: S	>8: R	<4: S	8
FOM	>16: R	>16: R	>16: R	>16: R	>16: R
LVFX	<2: S	<2: S	<2: S	4: S	>4: R
CPFX	<1: S	<1: S	<1: S	<1: S	>2: R

The score shows MIC (mg/ml) for *P. aeruginosa* (A–E). R indicates resistance and S indicates sensitive to *P. aeruginosa.* CAZ: ceftazidime hydrate; CFPM: cefepime hidrochloride hydrate; CPZ: cefoperazone sodium; IPM/CS: *imipenem/cilastatin sodium*; AZT: aztreonam; TOB: tobramycin; GM: Gentamicin sulfate; FOM: fosfomycin sodium; LVFX: levofloxacin hydrate; CPFX: Ciprofloxacin hydrochloride.

Table 2 Effect of cationic ions or FBS on MIC of AG30 or AG30/5C to *P. aeruginosa*

	AG30	AG30/5C
No treat	20	5
+1 mM $MgCl_2$	80	20
+3 mM $MgCl_2$	>80: R	>80: R
+6 mM $MgCl_2$	>80: R	>80: R
+1 mM $CaCl_2$	40	20
+3 mM $CaCl_2$	>80: R	>80: R
+6 mM $CaCl_2$	>80: R	>80: R
+10% FBS	>80:R	>80:R

The score shows MIC (mg/ml) for *P. aeruginosa.* R indicates resistance to *P. aeruginosa* (ATCC27853). FBS: foetal bovine serum.

successively through columns of Muromac (acetate form) and Sephadex G-10 using dilute acetic acid as an eluant, which was summarized in Figure 4B. We confirmed that the antibacterial and angiogenic functions of the peptides synthesized using the conventional solution method were similar to those synthesized by the previous solid method (data not shown). The advantages of this method include reduced synthesis cost and GMP grade applicability. Indeed, the cost to produce this peptide at a 10 g scale was roughly hundred thousand dollars, more than 10-fold reduction in price in comparison to the solid method. In addition, for GMP-scale procedures, each peptide-synthesis process is the same in the initial steps, and the final coupling reaction will be performed in the GMP facility. Based on this method, we will commence with large-scale production of this peptide for use in clinical trials.

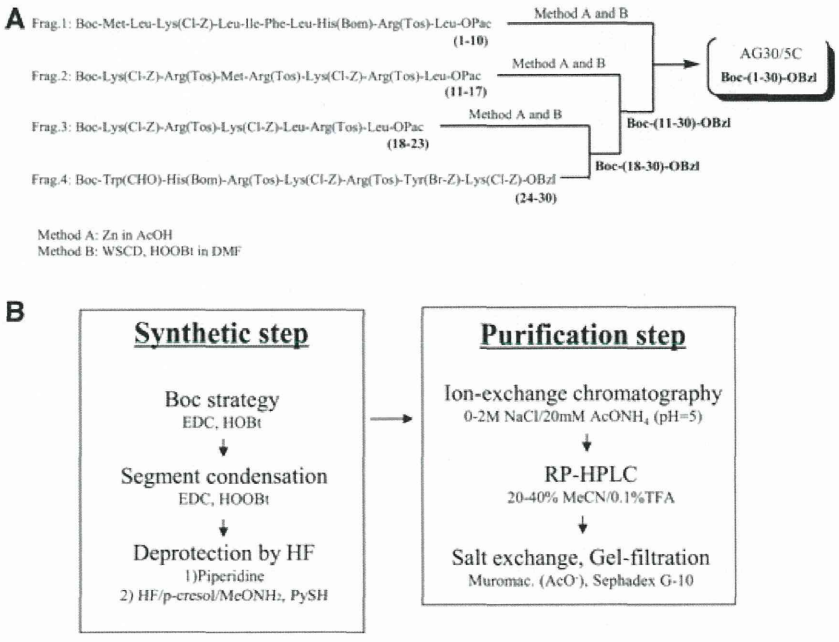

Fig. 4 The scheme for the synthesis of AG30/5C. (**A**) The AG30/5C molecule was assembled from four segments, that is (1–10), (11–17), (18–23) and (24–30), and each segment was elongated stepwise using the EDC/HOBt method as coupling reagents. (**B**) A large-scaled procedure employing the conventional solution method that is applicable for Good Manufacturing Practice toward clinical application in both synthetic and purification steps. The crude product was purified by ion-exchange chromatograpy followed by RP-HPLC. The purified product was passed successively through columns of Muromac and Sephadex G-10.

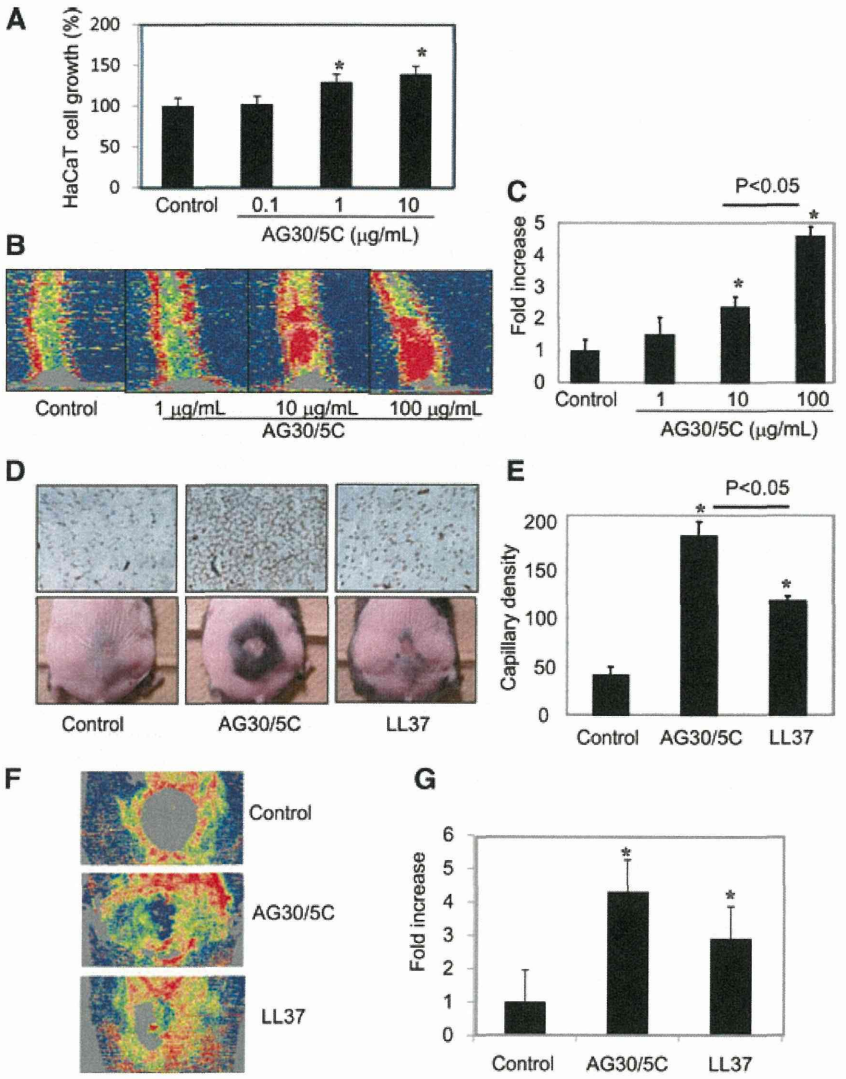

Fig. 5 Evaluation of the angiogenic effects of AG30/5C in a wound-healing model. (**A**) Cell growth of HaCaT cells in the presence of AG30/5C (0, 0.1, 1 and 10 μg/ml). The quantification is presented as a percent increase. $N = 8$ per group and duplicated. (**B**, **C**) Blood flow was analysed by Laser Doppler Image in mouse tails three days after induction of full thickness injuries with topical application of AG30/5C (0, 1, 10 and 100 μg/ml). Low or no perfusion is displayed as dark blue, whereas the highest perfusion interval is displayed as red; the quantification is presented as a fold increase. $N = 3$–5 per group and duplicated. $^*P < 0.05$ *versus* control. (**D**, **E**) Evaluation of wound healing in a diabetic mouse model treated with saline (control), AG30/5C or LL37. (**D**) The upper panel shows representative immunostains using anti-CD31 (PECAM) antibody (brown). The lower panel shows representative pictures after wound closure (day 24). Hair growth was observed around the edge of wound. (**E**) Capillary densities were quantified by cross section of ischaemic tissues immunostained with anti-CD31 (PECAM) antibody. $N = 6$–10 per group and duplicated. $^*P < 0.05$ *versus* control. (**F**, **G**) Blood flow was analysed by LDI in mouse wound 3 days after operation with topical application of AG30/5C (100 μg/ml). Low or no perfusion is displayed as grey or dark blue, whereas the highest perfusion interval is displayed as yellow or red; the quantification is presented as a fold increase. $N = 5$–6 per group and duplicated. $^*P < 0.05$ *versus* control.

We further examined the stability of this peptide in saline solution at both 5°C and room temperature. RP-HPLC analysis revealed that AG30/5C was fairly stable under 5°C for 12 months (96% stability), although it was less stable at room temperature (85% stability).

Effects of AG30/5C on murine and porcine wound models

In the process of wound healing, epidermal cell growth as well as angiogenesis is required to accelerate the time course of wound healing. Thus, we tested to examine the direct effect of AG30/5C on HaCaT cells. As shown in Figure 5A, the treatment of AG30/5C induced cell growth of HaCaT cells in a dose dependent manner. Thus, in the process of wound healing, AG30/5C can accelerate epithelialization as well as angiogenesis.

To evaluate the suitable dose of AG30/5C using a wound model [12], we measured the blood flow of mouse tails 3 days after inducing a full thickness injury. The topical application of AG30/5C at a dose of either 10 or 100 μg/ml significantly increased blood flow in a dose-dependent manner (Fig. 5B and C). Based on these results, we evaluated the angiogenic effects of AG30/5C and LL37 in a diabetic mouse wound-healing model. Capillary density within the ischaemic thigh adductor skeletal muscles was analysed to obtain specific evidence of vascularity at the level of the microcirculation [13, 14]. In the analysis of angiogenesis, microcapillary density was significantly increased

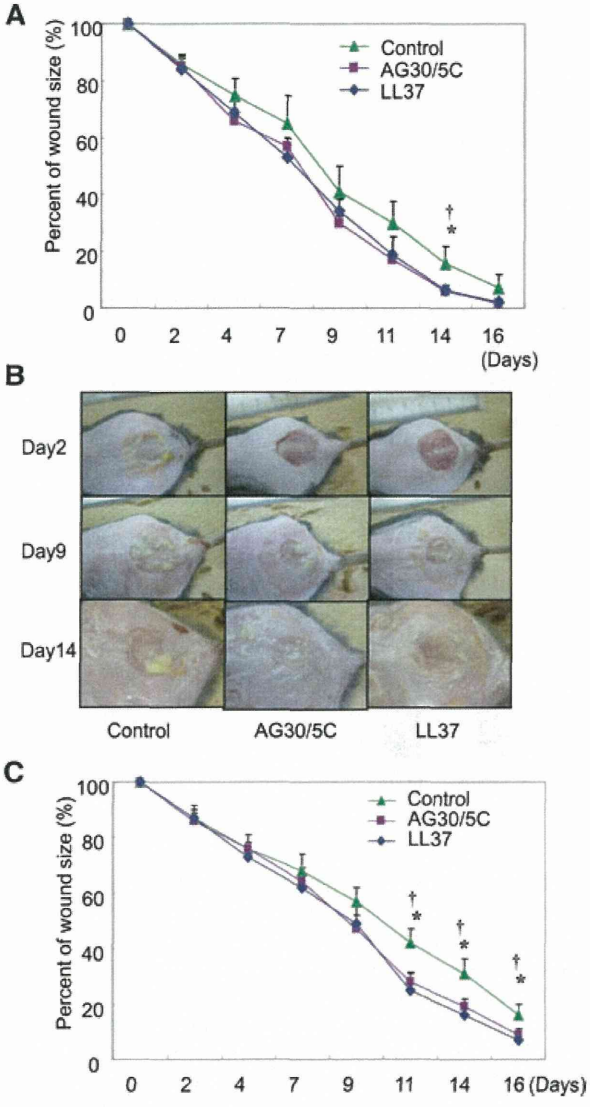

Fig. 6 Evaluation of the effects of AG30/5C in a diabetic mouse wound-healing model with or without MRSA infection. (**A**) Time course of the quantification of wound size in diabetic mice with treatment of saline (control), AG30/5C or LL37 (100 μg/ml, respectively). $N = 6$–10 per group and duplicated. $^{*}P < 0.05$ *versus* AG30/5C, $^{\dagger}P < 0.05$ *versus* LL37. (**B, C**) Evaluation of infectious wound healing in a diabetic mouse model treated with saline (control), modified AG30 or LL37. (**B**) Representative pictures of infectious wounds at days 2, 9 and 14. (**C**) Time course of the quantification of infectious wound size in diabetic mice treated with saline (control), AG30/5C or LL37 (100 μg/ml, respectively). $N = 5$–9 per group and duplicated. $^{*}P < 0.05$ *versus* AG30/5C, $^{\dagger}P < 0.05$ *versus* LL37.

in the AG30/5C-treated group in comparison to the LL37-treated group (Fig. 5D and E). Interestingly, at day 28 the hair growth was frequently observed in the AG30/5C-treated group (Fig. 5C). This result may support the angiogenic effects of AG30/5C because perifollicular angiogenesis undergoes a hair-cycle-dependent expansion and degeneration stage [20]. We further evaluated the angiogenic property of AG30/5C by measuring the blood flow just below the skin around wound. The evaluation of blood flow is also useful to examine an angiogenic effect [18]. As shown in Figure 5F and G, AG30/5C or LL37 treatment significantly increased the blood flow around the wound, compared with control group. These results illustrate the angiogenic properties of AG30/5C in wound-healing models.

Quantified analysis of the effect of AG30/5C in a wound-healing model

To investigate the possible clinical applications of AG30/5C, we quantified the effects of the peptide in a murine wound model. Under dressing conditions either with or without AG30/5C or LL37, the topical application of both compounds significantly decreased wound size at day 14 (Fig. 6A). Furthermore, three of the control-peptide-treated mice were afflicted with *S. aureus* infections during these experiments; in contrast, none of the mice in the AG30/5C- or LL37-treated groups became infected.

We also evaluated the antibacterial effects of AG30/5C using a murine infectious wound model. After topical treatment of MRSA on wounds, yellow pus was observed at day 2 and continuously increased over the duration of the experiment (Fig. 6B). We confirmed the presence of *S. aureus* in this yellow pus. Indeed, the infection delayed the time course of wound healing compared to a non-infectious wound-healing model. Importantly, co-treatment of either AG30/5C or LL37 attenuated the increase of yellow pus on the wounds (Fig. 6B) and significantly decreased wound size at days 11, 14 and 16 after treatment (Fig. 6C).

We further examined the effect of AG30/5C using a porcine wound model. After the topical application of both compounds every 2 days for 12 days under dressing condition, the diameter in the longitudinal views was evaluated as follows (control: 16.2 ± 0.5 mm, AG30/5C: 14.2 ± 0.5 mm, LL37: 15.4 ± 0.8 mm; Fig. 7A). In the evaluation of angiogenesis using a porcine wound model, microcapillary density was also significantly increased in both AG30/5C- and LL/37-treated groups in comparison to a control group (Fig. 7B and C). These results suggest that AG30/5C can potentially accelerate the wound-healing process.

Discussion

In this study, we modified a previously described functional peptide, AG30, in an effort to develop novel wound-healing drugs that could potentially be used for clinical applications. Historically, many microbial peptides have failed to prove effective in clinical applications; this is likely because such small peptides can be easily degraded by peptidases in addition to their short half-lives.

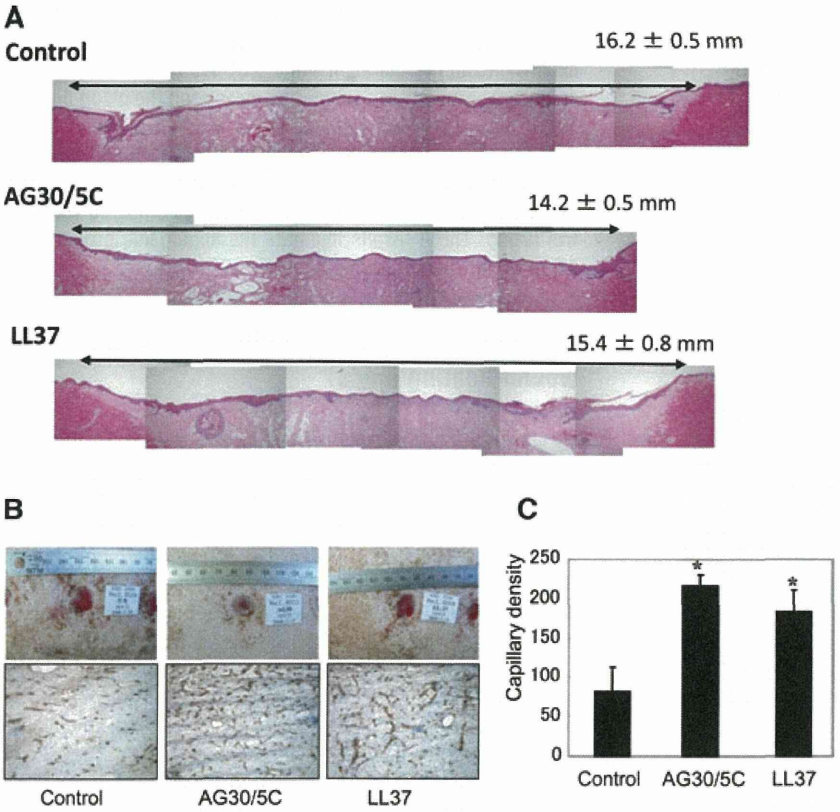

Fig. 7 Evaluation of the effects of AG30/5C on a porcine wound-healing model. (**A**) Representative pictures of haematoxylin and eosin staining on full-thickness section with restored epithelium, treated with saline (control), AG30/5C or LL37 (100 μg/ml, respectively). In the upper right corner, means ± S.E.M. (mm) were shown. (**B**) The upper panel shows representative pictures of wound healing in each group (day 9). The lower panel shows representative immunostains using anti-vWF antibody (brown). (**C**) Capillary densities were quantified by cross section of ischaemic tissue immunostained with anti-vWF antibody. $^{*}P < 0.05$ *versus* control. $N = 6$ per group and duplicated.

This study is a follow-up to a previous feasibility study aimed at generating lead compounds from a foundation compound.

Short cationic amphipathic peptides with antimicrobial and/or immunomodulatory activities are important components of the innate immune response and provide a template for two separate classes of antimicrobial drugs. Rapid acting and potent antimicrobial peptides are promising targets for investigation in the development of clinical treatments. In our modifications of the foundation peptide, we addressed the net positive charge and the amphipathic three-dimensional structure of AG30, and designed to modulate the balance between a net charge and α-helical structure by replacing a few amino acids. As a result, AG30/5C, replaced of five cationic amino acids, exhibited increased angiogenic and antimicrobial activities. Although AG30/5C showed the lowest ratio of α-helical the structure is still helical, and the three-dimentional structure of AG30/5C showed the broad cationic peptide surface. Thus, we speculate that AG30/5C can keep the cationic surface, which leads to increased activity, even though α-helical structure is not tightly fixed. Balancing these two parameters, thus enabling the net positive charged surface to attach and accumulate at the cell surface, was critical for the activity of this peptide. Indeed, the antibacterial action of this peptide was antagonized by the addition of divalent cations such as Mg^{2+} and Ca^{2+}. Some studies have modified antimicrobial peptides to develop new classes of antibiotics; however, this is the first report to modulate both antibacterial and angiogenic actions while maintaining activity and structure. The strategies and methods presented here could be useful in the further modifications of potential peptides in the early stages of clinical development.

Cationic antimicrobial peptides have a mixed history in clinical trials. The cationic peptides polymixin B and gramicidin S have long been used both in the clinic and as topical over-the-counter medicines. However, despite several clinical trials over the past ten years, the clinical success of cationic antimicrobial peptides has been limited [20]. To date, four cationic peptides have advanced into phase-III clinical trials. These peptides have been designed for treating impetigo and diabetic foot ulcers (the frog magainin derivative MSI-78; Pexiganan), oral mucosaitis (the pigprotegrin derivative IB-367; Iseganan), sepsis (the human bactericidal permeability protein derivative $rBPI_{23}$; Neuprex) and catheter-associated infections (the cattle indolicidin variant CP-226; Omiganan). Among them, Omiganan has achieved statistically significant success both in reducing infections that tunnel in from the catheter insertion site and in reducing catheter colonization during phase IIa trials [21]. Importantly, all four peptides are derivatives that were generated from original cationic peptides. Thus, in this study, we employed a feasibility study to develop lead compounds. Using an animal

wound-healing model, we utilized simple topical application without ointment or cream; this provided insight into the effectiveness of our peptide as a therapeutic drug and revealed some important limitations. To improve the effectiveness of the peptide as a therapeutic drug, it is possible that production of AG30/5C as an ointment or cream might enhance the local accumulation and structural stability of the peptide. The other aspect of peptide modification for eventual clinical development is to consider the cost of generating a peptide at the GMP level. In this study, we attempted to develop a large-scale procedure for the synthesis of AG30/5C that employed a conventional solution method applicable to Good Manufacturing Practice; importantly, we succeeded in generating a therapeutic peptide for use in pre-clinical trials. Furthermore, we tried to shorten the peptide while maintaining both its angiogenic and its antibacterial actions in an effort to minimize costs.

Based on these results, we have now transitioned into a pre-clinical study that includes evaluations of toxicity at single or repeated doses, genotoxicity and examination using local stimulation while monitoring serum concentrations of AG30/5C. We will continue to propose AG30/5C as a wound-healing drug for the treatment of ischaemic ulcers of diabetes patients or peripheral arterial diseases.

Acknowledgements

We thank all the members of the Gene Therapy Science Laboratory for critical discussions during the course of this work. We also thank Yuichi Koga and Kazufumi Takano in Department of Material and Life Science, Osaka University for technical help in CD analysis. This work was supported by the National Institute of Biomedical Innovation and the Takeda Science Foundation.

Conflict of interest

The authors declare no conflict of interest.

References

1. **Zasloff M.** Antimicrobial peptides of multicellular organisms. *Nature.* 2002; 415: 389–95.
2. **Hancock RE, Patrzykat A.** Clinical development of cationic antimicrobial peptides: from natural to novel antibiotics. *Curr Drug Targets Infect Disord.* 2002; 2: 79–83.
3. **Giangaspero A, Sandri L, Tossi A.** Amphipathic alpha helical antimicrobial peptides. *Eur J Biochem.* 2001; 268: 5589–600.
4. **Shai Y.** Mode of action of membrane active antimicrobial peptides. *Biopolymers.* 2002; 66: 236–48.
5. **Sorensen O, Bratt T, Johnsen AH, *et al.*** The human antibacterial cathelicidin, hCAP-18, is bound to lipoproteins in plasma. *J Biol Chem.* 1999; 274: 22445–51.
6. **Nishikawa T, Nakagami H, Maeda A, *et al.*** Development of a novel antimicrobial peptide, AG-30, with angiogenic properties. *J Cell Mol Med.* 2008; 13: 535–46.
7. **Rikitake Y, Hirata K, Kawashima S, *et al.*** Involvement of endothelial nitric oxide in sphingosine-1-phosphate-induced angiogenesis. *Arterioscler Thromb Vasc Biol.* 2002; 22: 108–14.
8. **Koczulla R, von Degenfeld G, Kupatt C, *et al.*** An angiogenic role for the human peptide antibiotic LL-37/hCAP-18. *J Clin Invest.* 2003; 111: 1665–72.
9. **Boman HG.** Antibacterial peptides: basic facts and emerging concepts. *J Intern Med.* 2003; 254: 197–215.
10. **Hunter HN, Jing W, Schibli DJ, *et al.*** The interactions of antimicrobial peptides derived from lysozyme with model membrane systems. *Biochim Biophys Acta.* 2005; 1668: 175–89.
11. **Jimenez MA, Evangelio JA, Aranda C, *et al.*** Helicity of alpha(404–451) and beta(394–445) tubulin C-terminal recombinant peptides. *Protein Sci.* 1999; 8: 788–99.
12. **Cho CH, Sung HK, Kim KT, *et al.*** COMP-angiopoietin-1 promotes wound healing through enhanced angiogenesis, lymphangiogenesis, and blood flow in a diabetic mouse model. *Proc Natl Acad Sci USA.* 2006; 103: 4946–51.
13. **Nakagami H, Maeda K, Morishita R, *et al.*** Novel autologous cell therapy in ischemic limb disease through growth factor secretion by cultured adipose tissue-derived stromal cells. *Arterioscler Thromb Vasc Biol.* 2005; 25: 2542–7.
14. **Kunigiza Y, Tomita N, Taniyama Y, *et al.*** Acceleration of wound healing by combined gene therapy of hepatocyte growth factor and prostacyclin synthase with Shima jet. *Gene Ther.* 2006; 13: 1143–52.
15. **D'Andrea LD, Iaccarino G, Fattorusso R, *et al.*** Targeting angiogenesis: structural characterization and biological properties of a *de novo* engineered VEGF mimicking peptide. *Proc Natl Acad Sci USA.* 2005; 102: 14215–20.
16. **Azuma J, Taniyama Y, Takeya Y, *et al.*** Angiogenic and antifibrotic actions of hepatocyte growth factor improve cardiac dysfunction in porcine ischemic cariomyopathy. *Gene Ther.* 2006; 13: 1206–13.
17. **Munoz V, Serrano L.** Elucidating the folding problem of helical peptides using empirical parameters. *Nat Struct Biol.* 1994; 1: 399–409.
18. **Petukhov M, Munoz V, Yumoto N, *et al.*** Position dependence of non-polar amino acid intrinsic helical propensities. *J Mol Biol.* 1998; 278: 279–89.
19. **Venyaminov S, Baikalov IA, Wu CS, *et al.*** Some problems of CD analyses of protein conformation. *Anal Biochem.* 1991; 198: 250–5.
20. **Yano K, Brown LF, Detmar M.** Control of hair growth and follicle size by VEGF-mediated angiogenesis. *J Clin Invest.* 2001; 107: 409–17.
21. **Zhang L, Falla TJ.** Antimicrobial peptides: therapeutic potential. *Expert Opin Pharmacother.* 2006; 7: 653–63.

A slow-releasing form of prostacyclin agonist (ONO1301SR) enhances endogenous secretion of multiple cardiotherapeutic cytokines and improves cardiac function in a rapid-pacing–induced model of canine heart failure

Tomonori Shirasaka, MD,[a] Shigeru Miyagawa, MD, PhD,[b] Satsuki Fukushima, MD, PhD,[b] Atsuhiro Saito, PhD,[b] Motoko Shiozaki, PhD,[b] Naomasa Kawaguchi, PhD,[c] Nariaki Matsuura, MD, PhD,[c] Satoshi Nakatani, MD, PhD,[d] Yoshiki Sakai, PhD,[e] Takashi Daimon, PhD,[f] Yutaka Okita, MD, PhD,[a] and Yoshiki Sawa, MD, PhD[b]

Objectives: Cardiac functional deterioration in dilated cardiomyopathy (DCM) is known to be reversed by intramyocardial up-regulation of multiple cardioprotective factors, whereas a prostacyclin analog, ONO1301, has been shown to paracrinally activate interstitial cells to release a variety of protective factors. We here hypothesized that intramyocardial delivery of a slow-releasing form of ONO1301 (ONO1301SR) might activate regional myocardium to up-regulate cardiotherapeutic factors, leading to regional and global functional recovery in DCM.

Methods and Results: ONO1301 elevated messenger RNA and protein level of hepatocyte growth factor, vascular endothelial growth factor, and stromal-derived factor-1 of normal human dermal fibroblasts in a dose-dependent manner in vitro. Intramyocardial delivery of ONO1301SR, which is ONO1301 mixed with polylactic and glycolic acid polymer (PLGA), but not that of PLGA only, yielded significant global functional recovery in a canine rapid pacing–induced DCM model, assessed by echocardiography and cardiac catheterization (n = 5 each). Importantly, speckle-tracking echocardiography unveiled significant regional functional recovery in the ONO1301-delivered territory, consistent to significantly increased vascular density, reduced interstitial collagen accumulation, attenuated myocyte hypertrophy, and reversed mitochondrial structure in the corresponding area.

Conclusions: Intramyocardial delivery of ONO1301SR, which is a PLGA-coated slow-releasing form of ONO1301, up-regulated multiple cardiotherapeutic factors in the injected territory, leading to region-specific reverse left ventricular remodeling and consequently a global functional recovery in a rapid-pacing–induced canine DCM model, warranting a further preclinical study to optimize this novel drug-delivery system to treat DCM. (J Thorac Cardiovasc Surg 2013;■:1-9)

ET/BS

Dilated cardiomyopathy (DCM) is characterized by progressive and severe deterioration of cardiac function, eventually leading to advanced heart failure necessitating surgical interventions such as cardiac transplantation[1] or mechanical assist device implantation,[2] despite maximum currently available medical therapy including angiotensin-converting enzyme inhibitor[3] or beta-blocker.[4] Despite a variety of etiologies in DCM, the diseases consistently include pathologic hypertrophy of cardiomyocytes associated with mitochondrial dysfunction, increased interstitial fibrosis, and limited regional blood flow.[5-7] Pathologic left ventricular (LV) remodeling is reportedly reversed, at least in part, by cell transplantation that intramyocardially up-regulates multiple cardiotherapeutic cytokines in a constitutive manner.[8,9] However, cell therapy is limited in the clinical arena owing to availability of cell processing center or ethical issues. Therefore, synthetic reagents that yield similar cardiotherapeutic effects to cell transplantation have been sought.

Prostacyclin is an endogenous factor released by endothelial cells, activating endothelial cells, fibroblasts, or smooth muscle cells in an autocrine and paracrine manner to release multiple growth factors or cytokines, consequently producing local and systemic anti-inflammatory, antifibrotic, proangiogenic, and antithrombotic effects. However, clinical use of synthetic prostacyclin or prostacyclin analogs, such as epoprostenol and beraprost, for chronic diseases is hampered by its chemical instability[10,11] and therefore the delivery method.

ONO1301 is a synthetic prostacyclin analog having a unique structural feature to maintain chemical stability,

From the Division of Cardiovascular Surgery,[a] Kobe University Graduate School of Medicine, Kobe; the Division of Cardiovascular Surgery,[b] Osaka University Graduate School of Medicine, Suita; the Department of Molecular Pathology,[c] Graduate School of Medicine and Health Sciences, Division of Functional Diagnostics,[d] Department of Health Sciences, Osaka University Graduate School of Medicine, Osaka; Ono Pharmaceutical Company Ltd,[e] Osaka; and the Division of Biostatistics,[f] Hyogo College of Medicine, Hyogo, Japan.

Disclosures: Yoshiki Sakai is an employee of ONO pharmaceutical Co Ltd. All other authors have nothing to disclose with regard to commercial support.

Received for publication July 27, 2012; revisions received Sept 8, 2012; accepted for publication Oct 2, 2012.

Address for reprints: Yoshiki Sawa, MD, PhD, Osaka University Graduate School of Medicine, Suita, Japan, E1: 2-2 Yamadaoka, Suita, Osaka 565-0871, Japan (E-mail: sawa@surg1.med.osaka-u.ac.jp).

0022-5223/$36.00

http://dx.doi.org/10.1016/j.jtcvs.2012.10.003

Abbreviations and Acronyms

DCM	= dilated cardiomyopathy
Dd	= end-diastolic left ventricular dimension
Ds	= end-systolic left ventricular dimension
E	= early transmitral filling wave
E′	= early diastolic velocity of the mitral annulus
EF	= ejection fraction
EDWT	= end-diastolic wall thickness
ELISA	= enzyme-linked immunosorbent assay
ESWT	= end-systolic wall thickness
HGF	= hepatocyte growth factor
LV	= left ventricular (ventricle)
mRNA	= messenger RNA
ONO1301SR	= slow releasing form of ONO1301
PCR	= polymerase chain reaction
PLGA	= polylactic and glycolic acid polymer
SDF-1	= stromal-derived factor-1
VEGF	= vascular endothelial growth factor

possibly allowing slow-releasing system.[12] Of note, ONO1301 reportedly activates fibroblasts to release multiple factors such as hepatocyte growth factor (HGF) and vascular endothelial growth factor (VEGF),[13] both of which are known to be cardiotherapeutic.[14,15] Nakamura and associates[13] reported that direct intramyocardial injection of ONO1301 yielded cardiotherapeutic effects in a model of acute myocardial infarction in the mouse. On the other hand, Hirata and colleagues[16] reported that subcutaneous injection of ONO1301 improves global cardiac function associated with globally reduced fibrosis and increased capillaries in a hamster DCM model. However, it remains unclear that intramyocardial delivery of ONO1301 would produce therapeutic effects on a model of DCM heart failure in a large animal.

We therefore hypothesized that intramyocardial injection of ONO1301 might activate regional interstitial cells including fibroblasts in the injected area to locally upregulate multiple therapeutic factors, leading to region-specific functional recovery in DCM. Thus, we investigated therapeutic effects of local administration of a slow-releasing form of ONO1301 on regional cardiac function of DCM heart by using the canine rapid-pacing induction that is an established DCM model.[17,18]

METHODS

Animal Care

All studies were performed with the approval of the institutional ethics committee in Osaka University Graduate School of Medicine. All animals were treated in compliance with the "Principles of Laboratory Animal Care" (the National Society for Medical Research) and the "Guide for the Care and Use of Laboratory Animals" (National Institutes of Health publication). Human dermal fibroblasts were treated in compliance with the principles outlined in the Declaration of Helsinki. All procedures and analysis were carried out in a blinded manner. We had full access to and take full responsibility for the integrity of data and agree to the manuscript as written.

Culture of Human Dermal Fibroblasts With ONO1301 Added

Human dermal fibroblast cell line (NHDF; CryoNHDF Neo, Lonza, Switzerland) was cultured in fine bubble mixing culture (FGM-2 Bulletkit, Lonza) containing 2% fetal bovine serum. ONO1301 (0.1-1.0 μmol/mL) was added for 72 hours after serum-free culture for 24 hours.

Generation of a Slow-Releasing Form of ONO1301

A slow releasing form of ONO1301 (ONO1301SR; Ono Pharmaceutical Co Ltd, Osaka, Japan) was created by polymerization of ONO1301 with polylactic and glycolic acid polymer (PLGA) as described previously.[19] In brief, ONO1301 (5 mg) was mixed with 100 mg of PLGA in 0.1% polyvinyl alcohol with an equal molar ratio of lactic acid/glycolic acid. Releasing time of ONO1301SR in vitro was between about 14 days to 25 days, as determined by measuring residual ONO1301 in the pellets by liquid chromatography.

Generation of Canine DCM Model and Intramyocardial ONO1301SR Injection

Beagles weighing 10 kg (Oriental Yeast Co Ltd, Tokyo, Japan) were endotracheally intubated and supported by mechanical ventilation under general anesthesia using intravenous sodium pentobarbitual (6 mg/kg) for induction and inhaled sevoflurane (1%-2%) for subsequent maintenance. We maintained the adequacy of anesthesia evaluated by giving the dogs electrical stimuli every 30 minutes. This evaluation was performed during each operation for each procedure. The heart was exposed via the left fifth intercostal space, and 2 bipolar pacing leads (FINELINE II EZ STEROX; Boston Scientific, Boston, Mass) were attached on the free wall of the right ventricle, connected to a pulse generator (INSIGNIA I, Boston Scientific) placed in subcutaneous pocket. The ventricle was continuously paced at 240 beats/min for 8 weeks.[18]

Four weeks after rapid pacing commenced, either ONO1301SR or PLGA polymer only was injected with a 26-gauge needle at 5 points of lateral wall of the LV at regular intervals (total 15 mg of ONO1301 or PLGA polymer was injected, ONO1301SR group and control group, n = 5 each). Rapid pacing was temporally discontinued during the injection procedure, and it was set back at 240 beats/min the day after each operation. Dogs kept on rapid pacing for 8 weeks were humanely killed under general anesthesia with an overdose of intravenous sodium pentobarbitual (18 mg/kg) to achieve complete sedation followed by administration of potassium-based solution intravenously to assure that they were completely dead. The hearts were retrieved at 4 weeks after injection of either ONO1301SR or PLGA only. We here defined lateral LV wall where ONO1301SR was directly injected as the "target site" and the septal wall as the "remote site."

Conventional and Speckle-Tracking Echocardiography and Cardiac Catheterization

Transthoracic echocardiography (Altida; Toshiba Medical Systems Corporation, Tochigi, Japan) was performed under general anesthesia by 1% sevoflurane inhalation. End-diastolic and end-systolic LV dimensions (Dd and Ds, respectively) and end-systolic and end-diastolic wall thickness (ESWT and EDWT, respectively) of the target site and remote site were measured at mid-LV short axis view by conventional echocardiography. LV ejection fraction (EF) was calculated with biplanar Simpson's rule

from the apical 4-chamber view. E/E′, an indicator of diastolic function, was calculated by measuring peak Doppler velocities of early transmitral filling wave (E) and the peak early diastolic velocity of the mitral annulus (E′).

Speckle-tracking echocardiography and an offline software (Altida Extend; Toshiba Medical Systems Corporation) were used to measure radial, circumferential, transverse, and longitudinal strains to quantitatively assess regional LV wall motion.[20] Radial and circumferential strains were measured from the mid-LV short-axis view, whereas transverse and longitudinal strains were from the apical 4-chamber view.

Cardiac catheterization was performed under general anesthesia using 1% sevoflurane inhalation. A 3F micromanometer-tipped catheter (SPR-249; Millar Instruments, Inc, Houston, Tex) was inserted through the LV apex to measure heart rate, LV maximal systolic pressure, maximal rate of the LV pressure change evaluating systolic preload-dependent LV function, and time constant of LV relaxation (τ) evaluating diastolic load-dependent function.

Real-Time Polymerase Chain Reaction

Total RNA was retrieved from NHDF by using RNeasy Mini kit (Qiagen, Venlo, The Netherlands) and treated with RNase-Free DNase Set (Qiagen). TaqMan probes were designed using Primer Express software (Applied Biosystems, Carlsbad, Calif). Real-time polymerase chain reaction (PCR) was performed using a 7500 Fast Real-Time PCR System with TaqMan Universal PCR Master Mix (Applied Biosystems). Concentration of HGF, VEGF, and stromal-derived factor-1 (SDF-1) in the culture supernatant of NHDF was measured by using an enzyme-linked immunosorbent assay (ELISA) kit (Procarta Cytokine Assay kit, Panomics, Santa Clara, Calif).

Histologic Analysis and Electron Microscopy

The extracted dog hearts were transversely cut, fixed with 10% buffered formalin, and embedded in paraffin. The heart sections of 10-μm thickness were stained with hematoxylin and eosin, Masson-trichrome, picro-sirius red, and periodic acid–Schiff. The heart sections were also labeled by anti-von Willebrand factor antibody (Dako EPOS) visualized by horseradish peroxidase (DakoCytomation, Glostrup, Denmark). Fibrotic area was calculated in the picro-sirius red–stained sections by using a planimetric method with a morphometry analyzer (NIS elements D, Nikon, Japan) on 5 optical fields that were selected randomly for each sample. Extracted dog heart tissues were fixed with 2.5% glutaraldehyde, stained with uranyl acetate and lead citrate, and examined with a Hitachi H-7100 electron microscope (Hitachi High-Technologies, Tokyo, Japan).

Statistical Analysis

All data are presented as the mean ± standard error of the mean. The analyses were performed using nonparametric methods because the sample sizes were too small to allow checking of the assumptions of parametric methods. Expression of messenger RNA (mRNA) in vitro analyzed by PCR and ELISA was analyzed by Jonckheere-Terpstra test for assuring dose-dependent effect of ONO1301. Hemodynamic data obtained from conventional echocardiography, cardiac catheterization, and speckle-tracking echocardiography, as well as histopathologic findings such as percent fibrosis, cell diameter, and vascular density at the target and remote sites of control group or ONO1301SR group, were analyzed by nonparametric repeated-measures analysis. Statistical analyses were performed with the R program (R Development Core Team 2011). R: A language and environment for statistical computing. R Foundation for Statistical Computing; Vienna, Austria).

RESULTS

Effects of ONO1301 on Expression of Endogenous Cytokines In Vitro

Effects of ONO1301 on expression of HGF, VEGF, and SDF-1 in the NHDF in vitro were examined by real-time PCR and ELISA. Relative expression of mRNA for HGF, VEGF, and SDF-1 was up-regulated in the NHDF with ONO1301 added in a dose-dependent manner (Figure 1, *A-C*), which was consistent with the release of HGF, VEGF, and SDF-1 into the supernatants (Figure 1, *D-F*).

Global Recovery of the DCM Heart by Injection of ONO1301SR

Serial changes in global systolic and diastolic cardiac function were assessed under general anesthesia by conventional echocardiography at 3 time points: 0 weeks (before commencement of rapid pacing), 4 weeks after the commencement of rapid pacing (just before injection of either ONO1301SR or PLGA only), and 4 weeks after injection of either ONO1301SR or PLGA only. Cardiac performance was markedly deteriorated, including increased Dd/Ds and E/E′ and decreased EF, ESWT, and EDWT at 4 weeks, when either ONO1301MS or PLGA only was intramyocardially injected.

At 4 weeks after PLGA injection, both systolic and diastolic cardiac functions had further deteriorated.

On the other hand, EF and ESWT/ EDWT at both the target site and remote site at 4 weeks after ONO1301SR injection were significantly greater than those at 4 weeks after PLGA injection (EF, 39% ± 1.7 % vs 19% ± 2.0%; $P < .05$; Figure 2, *E*; ESWT/EDWT at target site, $1.3 \pm 3.0 \times 10^{-2}$ vs $1.1 \pm 2.0 \times 10^{-2}$; $P = .01$; Figure 2, *C*; ESWT/EDWT at remote site, 1.2 ± 0.1 vs $1.1 \pm 3.0 \times 10^{-2}$; $P = .04$; Figure 2, *D*), although the impact of the recovery was stronger in the target site. Ds was significantly smaller after ONO1301SR injection than after PLGA injection (Ds, 23 ± 2.4 vs 31 ± 1.7 mm; $P < .05$; Figure 2, *B*), whereas Dd also showed a trend to be smaller after ONO1301SR injection than after PLGA injection (Dd, 29 ± 2.3 vs 34 ± 1.4; $P < .05$; Figure 2, *A*). E/E′ after ONO1301SR injection was significantly smaller than that after PLGA injection (E/E′, 11 ± 1.2 vs 16 ± 0.5; $P < .05$; Figure 2, *F*).

Cardiac catheterization, carried out at 4 weeks after either ONO1301SR or PLGA injection, revealed that τ was significantly smaller after ONO1301SR injection than after PLGA injection (τ, 32 ± 0.9 vs 55 ± 5.8; $P < .05$). Heart rate, LV maximal systolic pressure, and maximal rate of the LV pressure change did not show any significant difference at 4 weeks after injection of either ONO1301SR or PLGA.

Regional Functional Recovery After ONO1301SR Injection

Serial changes of regional systolic cardiac function were assessed under general anesthesia by speckle-tracking echocardiography at the same 3 time points as conventional echocardiography. At 4 weeks after the commencement of rapid pacing, all strain values at both target and remote sites were decreased compared with those

ET/BS

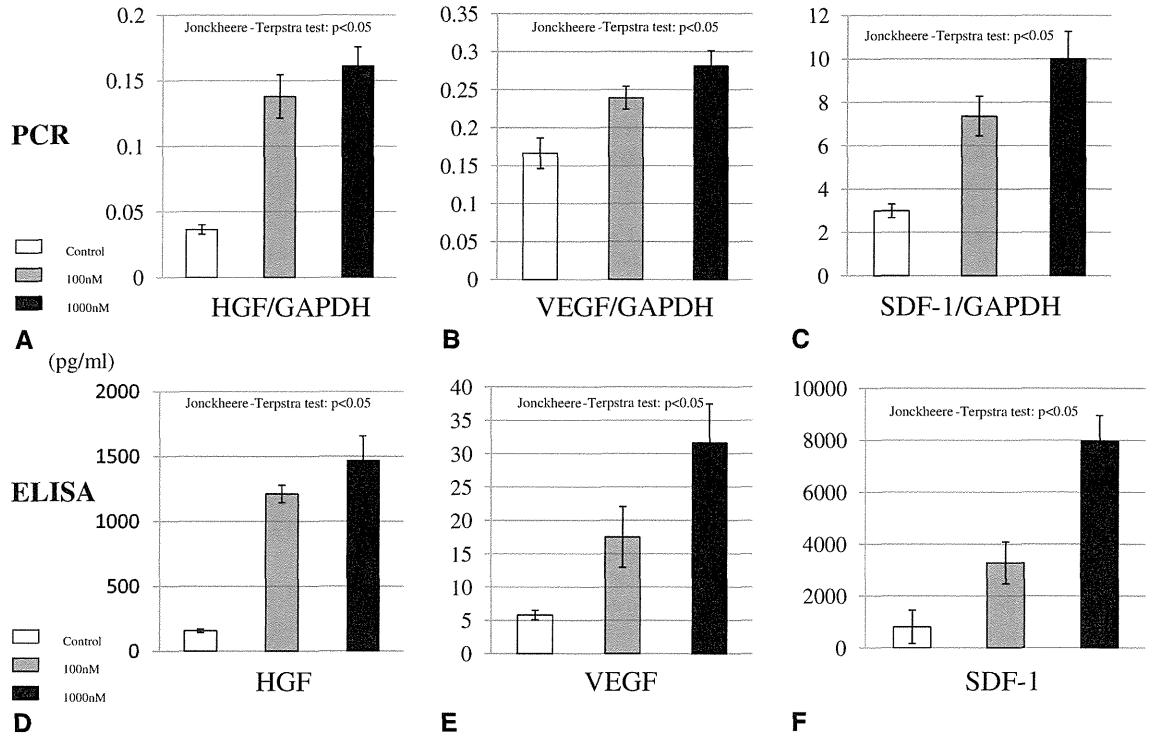

FIGURE 1. PCR and ELISA analysis in vitro showed that messenger RNA levels for HGF (A and D), VEGF (B and E), and SDF-1 (C and F) increased in a dose-dependent manner in NHDF cultured with ONO1301. *PCR*, Polymerase chain reaction; *ELISA*, enzyme-linked immunosorbent assay; *NHDF*, normal human dermal fibroblast; *HGF*, hepatocyte growth factor; *GAPDH*, glyceraldehyde-3-phosphate dehydrogenase; *SDF-1*, stromal-derived factor-1; *VEGF*, vascular endothelial growth factor. Mean ± standard error of the mean, respectively.

before rapid pacing. At 4 weeks after the PLGA injection, the absolute values of peak systolic radial, circumferential, transverse, and longitudinal strains at both target and remote sites further decreased compared with those before the PLGA injection. In contrast, at 4 weeks after the ONO1301SR injection, strain values of radial, transverse, and circumferential strains were greater at the target site than those after the PLGA injection (radial strain, 36% ± 4.7% vs 8.3% ± 1.4%; $P < .05$; transverse strain, 39% ± 9.3% vs 9.5% ± 2.1%; $P < .05$; circumferential strain, −11% ± 1.3% vs −3.9% ± 0.6%; $P < .05$; Figure 3, *A-C*), although longitudinal strain was not different between the hearts with and without ONO1301SR treatment (Figure 3, *D*). On the other hand, only radial strain was significantly improved at the remote site after ONO1301SR injection compared with that after PLGA injection (Figure 3, *E-H*).

Histologic Findings of Reverse LV Remodeling After ONO1301SR Injection

Gross myocardial structure, assessed by hematoxylin and eosin staining and Masson trichrome staining, showed a thicker LV wall and a smaller LV cavity 4 weeks after ONO1301SR administration (Figure 4, *H-K*) than that after PLGA injection (Figure 4, *D-G*).

Quantity of interstitial fibrosis at the target site, evaluated by picro-sirius red staining, was significantly less at 4 weeks after ONO1301SR administration compared with that after PLGA injection (percent fibrosis at the target site, 9.9% ± 0.7% vs 23% ± 0.9%; $P < .01$; Figure 4, *A*). Of note, distribution of interstitial fibrosis was significantly more restricted at the target site than that at the remote site after ONO1301SR administration (9.9% ± 0.7% vs 16% ± 1.2%), whereas PLGA injection did not produce such an uneven distribution (23% ± 0.9% at the target site vs 23% ± 0.8% at the remote site).

Mean transverse cellular diameter of cardiomyocytes (Figure 4, *B*) at the target site, measured by periodic acid-Schiff–stained sections, was also significantly smaller at 4 weeks after ONO1301SR administration compared with that after PLGA injection (12 ± 0.6 mm vs 15 ± 0.8 mm; $P < .01$). The diameter of cardiomyocytes at the target site was smaller after ONO1301SR administration compared with that at the remote site (12 ± 0.6 vs 14 ± 0.3 mm; $P < .01$), whereas such an uneven distribution in the myocyte size was not observed after PLGA injection.

Vascular density (Figure 4, *C*), assessed by counting the number of factor VIII–positive cells in the fields, was significantly greater at the target site at 4 weeks after ONO1301SR administration compared with that after

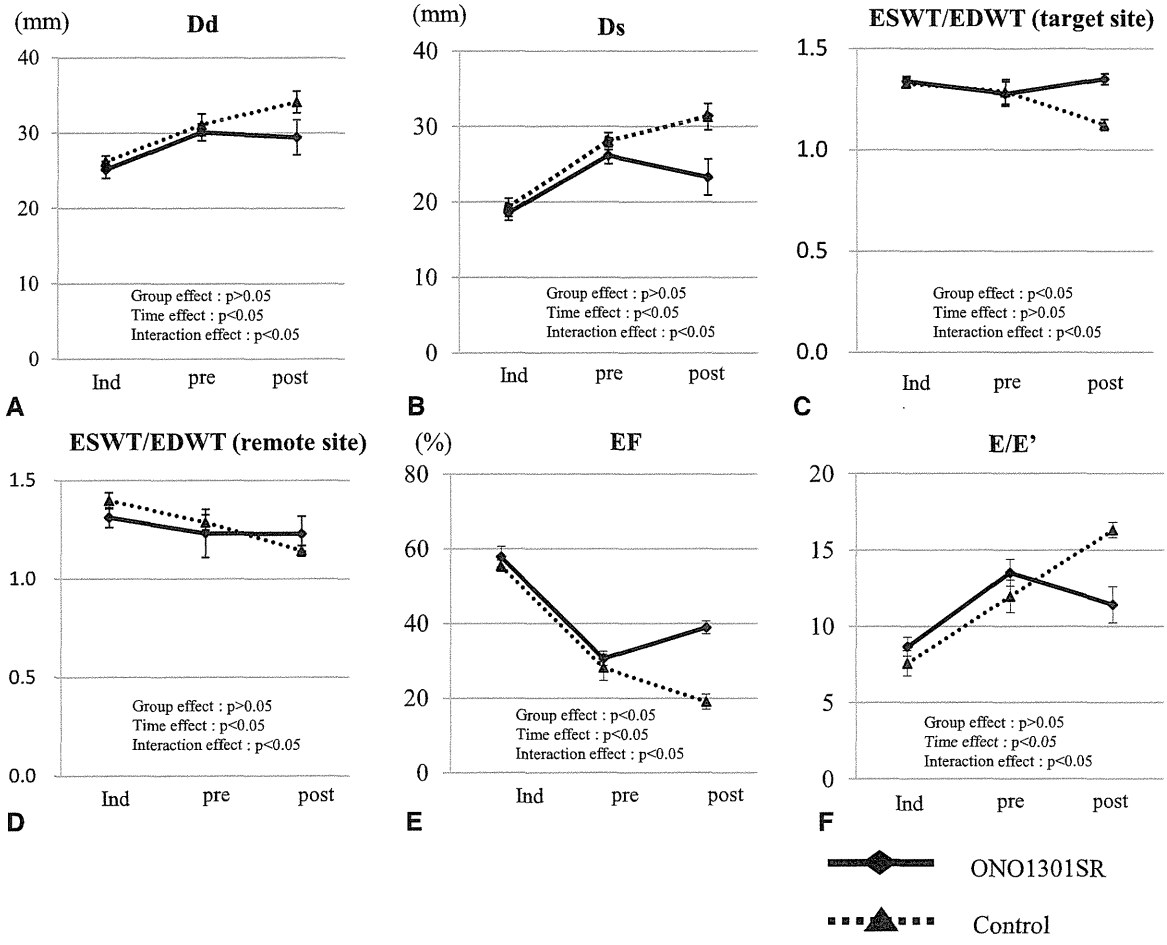

FIGURE 2. Echocardiography (A-F) showed ONO1301SR significantly improved distressed cardiac function. Note that ESWT/EDWT, reflecting on the radial strain of myocardium, was significantly more recovered in the ONO1301SR group than in the control group and that the clinical impact was more prominent in the target site after ONO1301SR treatment. *Dd*, End-diastolic dimension of the left ventricle; *Ds*, end-systolic dimension of the left ventricle; *EF*, ejection; *ESWT*, end-systolic wall thickness; *EDWT*, end-diastolic wall thickness. Mean ± standard error of the mean, respectively. *Ind*, induction of rapid pacing; *Pre*, before treatment of polylactic and glycolic acid polymer *(PLGA)* or ONO1301SR; *Post*, after treatment of PLGA or ONO1301SR.

PLGA injection ($998 \pm 70/mm^2$ vs $467 \pm 33/mm^2$; $P < .01$). The vascular density at the target site was greater after ONO1301SR administration compared with that at the remote site ($998 \pm 70/mm^2$ vs $491 \pm 24/mm^2$), whereas such an uneven distribution of vascular density was not observed after PLGA injection.

Electron microscopy revealed that the cardiomyocytes at 4 weeks after PLGA injection showed a prominent swelling or disruption of mitochondria, intracellular or perinuclear edema, and sarcoplasmic vacuoles resulting from dilation of sarcoplasmic reticulum (Figure 5, *A*). However, marked loss of myofilaments and alterations of characteristic sarcomeric structure were not observed in any groups. Although the interfibrillar space in the myocardium after ONO1301SR injection was slightly widened, the mitochondria were compact and showed densely packed cristae (Figure 5, *B*) compared with those after PLGA injection.

DISCUSSION

We here demonstrate that ONO1301 dose-dependently up-regulated expression of multiple cytokines, such as HGF, VEGF, and SDF-1, in fibroblasts in vitro. Histologic reverse LV remodeling, such as attenuated fibrosis and swelling of cardiomyocytes, increased vascular density, and recovered mitochondrial structure, in the target area but not significantly in the remote area, were consistent to the regional functional recovery, assessed by speckle-tracking echocardiography, which was more prominent at the target area than that at the remote area after the ONO1301SR injection. Such regional recovery at the target area after ONO1301SR injection resulted in recovery of global function, including systolic and diastolic function.

Iwata and associates[21] reported that local administration of prostacyclin analog may induce HGF production followed by VEGF expression via cyclic adenosine monophosphate–mediated pathway and that elevation of HGF

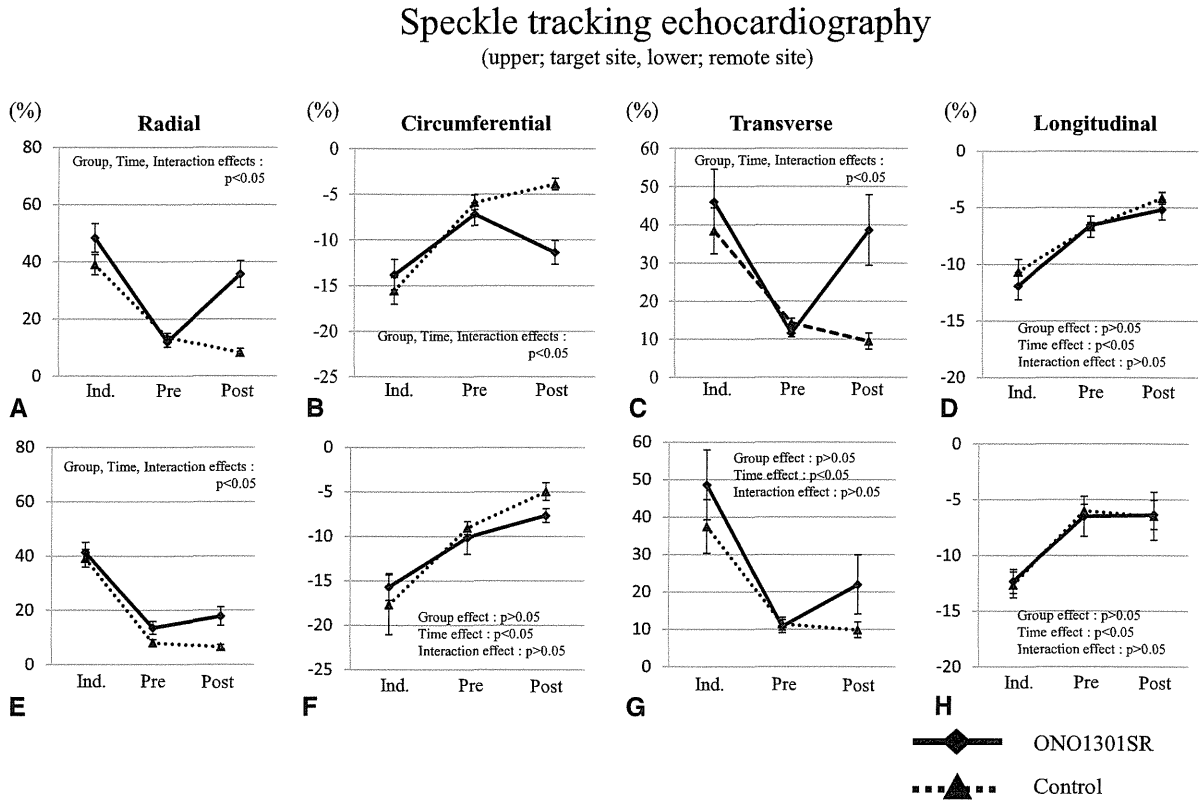

FIGURE 3. Speckle-tracking echocardiography showed that the absolute values of peak radial, circumferential, and transverse strains at the target site in the ONO1301SR group were significantly higher than in the control group (A-D) while all of them but radial strains at the remote site in the ONO1301SR group and that in the control group were not significantly different (E-H), which implied that ONO1301SR had influence on the cardiac performance especially at the very site where ONO1301SR was administered; *Radial*, radial strain; *Circumferential*, circumferential strain; *Transverse*, transverse strain; *Longitudinal*, longitudinal strain. Target site is defined as the area in which ONO1301SR or glycolic acid polymer *(PLGA)* is injected while remote site as noninjection area. *Ind*, Induction of rapid pacing; *Pre*, before treatment of PLGA or ONO1301SR; *Post*, after treatment of PLGA or ONO1301SR. Mean ± standard error of the mean, respectively.

or VEGF may mediate the favorable effect in the treatment of ischemic heart failure. We here showed that ONO1301 directly activates fibroblasts in vitro and releases not only HGF and VEGF, as reported previously,[13,16,21] but also SDF-1, which has been thought to be a representative therapeutic stem cell homing factor in ischemic heart.[22] In the present in vivo study, we used the slow-releasing form to deliver ONO1301 and, importantly, deliver ONO1301SR directly into the myocardium of the canine DCM heart in the aim to elevate regionally ONO1301 level, thus maximizing the effects on the cardiac fibroblasts to release cardiotherapeutic factors. Consequently, pathologic and functional effects of intramyocardial ONO1301SR injection were markedly prominent in the target area (area surrounding the injection sites) compared with the remote area, suggesting that cardiac fibroblasts residing in the target area might have played a key role in locally up-regulated cardiotherapeutic cytokines.

In addition, it was noted that the typical structural features of cardiomyocytes in the severely ischemic heart, such as swelling of mitochondria, intracellular or perinuclear edema, and sarcoplasmic vacuoles referred to by a phenomenon, "permeability transition,"[23] were reversed after ONO1301SR injection in this study. On the basis of these findings, targeted injection of ONO1301SR into the damaged myocardial area might maximize therapeutic effects of ONO1301 that up-regulates cardiotherapeutic cytokines in a regional concentration-dependent manner.

Use of slow releasing form in administrating ONO1301 directly into the heart includes concerns related to the initial burst that might have an adverse effect on hemodynamics.[24] In this study, there is no hemodynamic compromise during or immediately after the procedure despite the poor cardiac function, suggesting that the protocol used here in injecting ONO1301SR might be appropriate in treating the DCM heart. Further study for dose-dependent hemodynamic change immediately after ONO1301SR administration would be needed in translating this treatment into the clinical arena.

Intramyocardial delivery of ONO1301 might be achieved by direct injection, intracoronary artery injection,

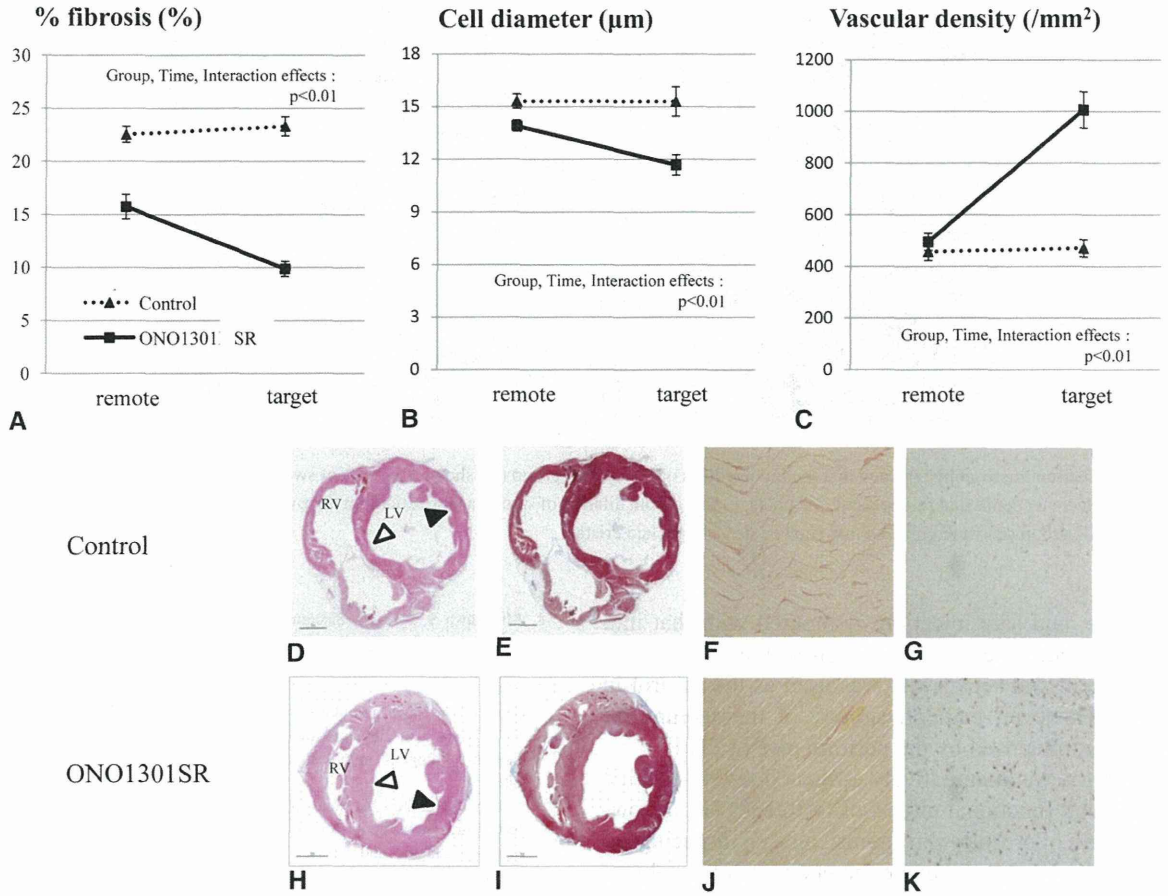

FIGURE 4. Histopathology; quantitative evaluation of interstitial fibrosis (A), mean cell diameter (B), vascular density (C), and representative micrograph of the Control group (D-G) and the ONO1301SR group (H-K). D and H, Hematoxylin and eosin staining. E and I, Masson trichrome staining. F and J, Sirius red staining. G and K, Staining with anti-human-von Willebrand factor. At the target site in the ONO1301SR group, the amounts of fibrosis and mean cell diameter were significantly smaller and vascular density was significantly higher than those in the control group and those at the remote site in the ONO1301SR group. Mean ± standard error of the mean, respectively. *LV*, Left ventricle; *RV*, right ventricle.

or attachment on the epicardial surface. Injection area–specific recovery, demonstrated in this study, would suggest that direct injection of ONO1301 might be more effective in the myocardium that has heterogeneous disease, such as ischemic cardiomyopathy, as reported by Iwata and associates.[21] Combination with coronary artery bypass grafting would also be a clinically applicable strategy for this purpose. On the other hand, homogeneous disease such as DCM might gain more therapeutic benefits by diffusely attaching ONO1301 on the epicardial surface compared with direct injection, although further basic investigation will be needed to establish this strategy. Intracoronary injection is known to diffusely deliver reagents or cells into the myocardium[25]; however, intracoronary injection of ONO1301SR whose diameter is more than 20 μm will cause coronary embolism and ischemic myocardial damage.

This study is limited by the use of a canine model, which is not exactly relevant to the clinical DCM diseases and has limited reagents for mRNA or protein investigations available.

However, a large animal model is essential in investigating cardiac performance by the latest technology used in the clinical arena, such as speckle-tracking echocardiography used in this study, whereas rodent models with or without genetic modifications would be useful in showing the mechanistic insights of this treatment. As mechanistic insights have been reported by several studies, the main focus of this study was to test the hypothesis that intramyocardial injection of ONO1301 induces region-specific and global functional recovery in dilated cardiomyopathy. In addition, this study investigated the mechanisms of this treatment to show the consistency with the previous studies that used rodent models to prove the mechanisms of this treatment.

Injection to the anterior wall and use of the posterior wall as the control was an option; however, in the surgical view, injection into the lateral wall produced consistent,

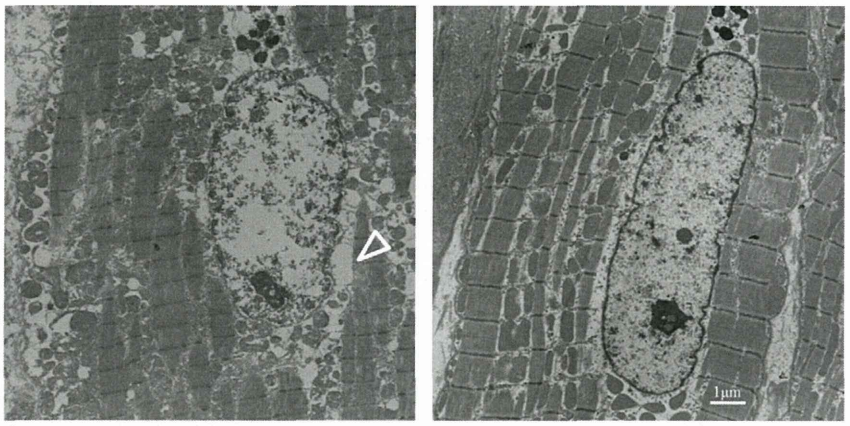

FIGURE 5. Electron microscopy revealed that the myocardium of the control group (A) showed prominent swelling or disruption of mitochondria, intracellular or perinuclear edema, and sarcoplasmic vacuoles resulting from dilation of sarcoplasmic reticulum *(arrowhead)*. On the other hand, mitochondria in the ONO1301SR group (B) were compact and showed densely packed cristae.

reproducible, and safe injections compared with that into the anterior wall. Therefore, injection of the reagent into the lateral wall and septal wall was used as the control in this study. However, pathophysiology of the septum are substantially influenced by the performance of the RV.

In summary, we quantitatively evaluated region-specific pathologic and functional effects of ONO1301SR, a slow-releasing form of prostacyclin agonist, on a rapid-pacing canine DCM model. Multitherapeutic endogenous cytokines induced by intramyocardial ONO1301SR injection may be responsible for the improved cardiac performance and ultrastructure. ONO1301SR is a promising therapeutic drug for enhancing myocardial regeneration on the impaired myocardium.

We thank Masako Yokoyama, Yuka Fujiwara, and Shigeru Matsumi for their excellent technical assistance.

References

1. Sharon AH, François H. The changing face of heart transplantation. *J Am Coll Cardiol*. 2008;52:587-98.
2. Maybaum S, Mancini D, Xydas S, Starling RC, Aaronson K, Pagani FD, et al. Cardiac improvement during mechanical circulatory support: a prospective multicenter study of the LVAD working group. *Circulation*. 2007;115:2497-525.
3. Cohn JN, Tognoni G, for the Valsartan Heart Failure Trial Investigators. A randomized trial of the angiotensin-receptor blocker valsartan in chronic heart failure. *N Engl J Med*. 2001;345:1667-75.
4. Packer M, Bristow MR, Cohn JN, Coluggi WS, Fowler MB, Gilbert EM, et al. The effect of carvedilol on morbidity and mortality in patients with chronic heart failure. *N Engl J Med*. 1996;334:1349-55.
5. Lesnefsky EJ, Moghaddas S, Tandler B, Kerner J, Hoppel CL. Mitochondrial dysfunction in cardiac disease: ischemia–reperfusion, aging, and heart failure. *J Mol Cell Cardiol*. 2001;33:1065-89.
6. Schaper J, Froede R, Hein S, Buck A, Hashizume H, Speiser B, et al. Impairment of the myocardial ultrastructure and changes of the cytoskeleton in dilated cardiomyopathy. *Circulation*. 1991;83:504-14.
7. Unverferth DV, Baker PB, Swift SE, Chaffee R, Fetters JK, Uretsky BF, et al. Extent of myocardial fibrosis and cellular hypertrophy in dilated cardiomyopathy. *Am J Cardiol*. 1986;57:816-20.
8. Miyagawa S, Saito A, Sakaguchi T, Yoshikawa Y, Yamauchi T, Imanishi Y, et al. Impaired myocardium regeneration with skeletal cell sheets—a preclinical trial for tissue-engineered regeneration therapy. *Transplantation*. 2010;90:364-72.
9. Memon IA, Sawa Y, Fukushima N, Matsumiya G, Miyagawa S, Taketani S, et al. Repair of impaired myocardium by means of implantation of engineered autologous myoblast sheets. *J Thorac Cardiovasc Surg*. 2005;130:646-53.
10. Sitbon O, Humbert M, Nunes H, Parent F, Garcia G, Simonzeau G, et al. Long-term intravenous epoprostenol infusion in primary pulmonary hypertension: prognostic factors and survival. *J Am Coll Cardiol*. 2002;40:780-8.
11. Barst RJ, McGoon M, McLaughlin V, Tapson V, Oudiz R, Shapiro S, et al. Beraprost therapy for pulmonary arterial hypertension. *J Am Coll Cardiol*. 2003;41:2119-25.
12. Kataoka M, Nagaya N, Satoh T, Itoh T, Murakami S, Iwase T, et al. A long-acting prostacyclin agonist with thromboxane inhibitory activity for pulmonary hypertension. *Am J Respir Crit Care Med*. 2005;172:1575-80.
13. Nakamura K, Sata M, Iwata H, Sakai Y, Hirata Y, Kugiyama K, et al. A synthetic small molecule, ONO-1301, enhances endogenous growth factor expression and augments angiogenesis in the ischaemic heart. *Clin Sci (London)*. 2007;112:607-16.
14. Taniyama Y, Morishita R, Aoki M, Hiraoka K, Yamasaki K, Hashiya N, et al. Angiogenesis and antifibrotic action by hepatocyte growth factor in cardiomyopathy. *Hypertension*. 2002;40:47-53.
15. Van Belle E, Witzenbichler B, Chen D, Silver M, Chang L, Schwall R, et al. Potentiated angiogenic effect of scatter/hepatocyte growth factor via induction of vascular endothelial growth factor: the case for paracrine amplification of angiogenesis. *Circulation*. 1998;97:381-90.
16. Hirata Y, Soeki T, Akaike M, Sakai Y, Igarashi T, Sata M. Synthetic prostacycline agonist, ONO-1301, ameliorates left ventricular dysfunction and cardiac fibrosis in cardiomyopathic hamsters. *Biomed Pharmacol*. 2009;63:781-6.
17. Armstrong PW, Stopps TP, Ford SE, DeBold AJ. Rapid ventricular pacing in the dog: pathophysiologic studies of heart failure. *Circulation*. 1986;74:1075-84.
18. Hata H, Matsumiya G, Miyagawa S, Kondoh H, Kawaguchi N, Matsuura N, et al. Grafted skeletal myoblast sheets attenuate myocardial remodeling in pacing-induced canine heart failure model. *J Thorac Cardiovasc Surg*. 2006;132:918-24.
19. Obata H, Sakai Y, Ohnishi S, Takeshita S, Mori H, Kodama M, et al. Single injection of a sustained-release prostacyclin analog improves pulmonary hypertension in rats. *Am J Respir Crit Care Med*. 2008;177:195-201.
20. Ogawa K, Hozumi T, Sugioka K, Matsuyama Y, Nishiura M, Kanda R, et al. Usefulness of automated quantification of regional left ventricular wall motion by a novel method of two-dimensional echocardiographic tracking. *Am J Cardiol*. 2006;98:1531-7.

21. Iwata H, Nakamura K, Sumi M, Ninomiya M, Sakai Y, Hirata Y, et al. Local delivery of synthetic prostacycline agonist augments collateral growth and improves cardiac function in a swine chronic cardiac ischemia model. *Life Sci.* 2009;85:255-61.
22. Effect of stromal-cell-derived factor 1 on stem-cell homing and tissue regeneration in ischaemic cardiomyopathy. *Lancet.* 2003;362:697-703.
23. Weiss JN, Korge P, Honda HM, Ping P. Role of the mitochondrial permeability transition in myocardial disease. *Circ. Res.* 2003;93:292-301.
24. Hazekawa M, Sakai Y, Yoshida M, Haraguchi T, Morisaki T, Uchida T. Preparation of ONO-1301-loaded poly (lactide-co-glycolide) microspheres and their effect on nerve conduction velocity. *J Pharm Pharmacol.* 2011; 63:362-8.
25. Fukushima S, Varela-Carver A, Coppen SR, Yamahara K, Felkin LE, Lee J, et al. Direct intramyocardial but not intracoronary injection of bone marrow cells induces ventricular arrhythmias in a rat chronic ischemic heart failure model. *Circulation.* 2007;115:2254-61.